ARCHIVES OF ACOUSTICS
8, 4, 271-292 (1983)

ANALYSIS OF THE SPECIFIC STRUCTURE OF THE FUNDAMENTAL COMPONENT OF VOCAL SOUNDS FROM THE POINT OF VIEW OF INTONATION EVALUATION

HELENA HARAJDA

Pedagogical University (65-069 Zielona Góra, Plac Słowiański 6)

Finding it necessary to develop the acoustic basis for the evaluation of the correctness of vocal sound intonation, with consideration given to the clarity of intonation, the correctness of pitch attack and pitch stabilization, investigations were performed on the formation in the process of intonation of an isolated sound, of parameters of the fundamental component which provide information about the deep structure of this sound. The method of intonographic plotting was used and statistical calculations performed. The following quantities were considered: the duration of an isolated sound over one breath (t), the formation time of the amplitude and frequency of the fundamental component of an isolated, freely intoned sound (τ_A, τ_F), the value and variation of the amplitude level (A and ΔA), the fidelity of standard frequency reproduction and frequency variation (σ, ν) within the limits of the quasi-steady state of sound. The investigations were performed on three groups of children and one of adolescents (20 voices in all).

The results obtained have led to the conclusion that there are distinct differences in the deep structure of the fundamental component of isolated sounds intoned by the different age groups. These differences can constitute a physical basis for evaluating the ability to intone vocal sounds.

1. Introduction

Vocal sounds are outstanding among music sounds, since they not only constitute the basic artistic material, but are also the most frequent standard. Knowledge of their specific structure is necessary for developing objective criteria which are equivalent to factors considered in subjective evaluation affecting the correctness of intonation, which continues to be the object of evaluation in the process of music education. Research on sound intonation problems has mainly been centred on the sounds of bow instruments [9], [12], Part of the problems considered in this research has also been concerned with vocal intonation. The so-called component tones of sound, included in the composition of the spectral structure of music sounds, are not homogeneous in

terms of their characteristic parameters, both in reference to vocal and violin sounds. Over the range of individual sounds, both the frequency and amplitude vary continuously in time, forming a sort of complex substructure [7]. In order to distinguish it from the spectral structure, in the present paper it is called a "specific" or "deep" structure. The central problem in working towards objectivization of the process of evaluation of intonation correctness is selecting factors responsible for its quality — such factors which are perceptible by the ear and have their equivalents among the acoustic structural elements of sound. WROŃSKI [17] took GARBUZOV'S theory [5] as the basis of theoretical evaluation of intonation. This theory can be the starting point in evaluating the agreement between the desired sound pitch and the pitch assumed as the standard, being closely related to the frequency. Correctness of intonation is determined not only by the fidelity of standard reproduction but also a number of other factors play their role. LESMAN [8] drew attention to intonation certainty, which is related to variation in the pitch of a given sound as it lasts. FLESCH [3] considered the problem of the possibility of correcting pitch over the time of sound formation, the so-called sound attack. TJERNLUND [16], on the basis of the results of computer research and statistical calculations of sound parameters, drew attention to the intonation deviation of the fundamental frequency during playing. BJÖRKLUND [1] already took into consideration variations of parameters which occur within individual sounds and studied the significance of vibrato in the process of intonation in untrained voices. RAGS [13] and RAKOWSKI [14] considered the effect of vibrato on the evluation of sound pitch. All the factors mentioned above are related to the formation of sound structure, spectral [15] or deep [4]. The problem of the correctness of the structure of vocal sounds intoned is particularly complex in the case of children's voices, in view of the differentiation of vocal activity among children of different age [10].

The purpose of the research described in this paper was to define the deep structure of the first component of sound which is equivalent to the theoretical fundamental tone (called the fundamental component below) of sounds intoned by children and adolescents. This problem was considered in terms of analysis of the possibility of assuming individual elements of the structure as the basis for evaluating intonation correctness.

2. Organization and technique of the investigations

The investigations were performed on voices from three age groups of children: 7-8 years, 9-11 years and 12-14 years and adolescent voices of one group of students (from the course of music education in Pedagogical University Zielona Góra), with five persons in each group, 20 persons in all.

The children were secondary school pupils, physically and mentally normal (doctor's and psychologist's data files having been consulted); they had good

results in learning, in general and in music classes. Their music education was limited to a course in secondary school. All the children worked under supervision of a qualified teacher, an expert in music education.

The adolescent group was composed of average musically gifted persons, without professional vocal training.

All the groups underwent audiometric examination. No essential hearing loss, i.e. over 30 dB, was found.

The persons selected for the investigations underwent training consisting in a test session, combined with necessary instructions regarding the technique of recordings.

The recordings were made in a damped booth, under constant teacher supervision. The intoning persons sat in an armchair, which limited head movements. It was found at preliminary sessions, on the basis of sound intensity level measurements, that during intoning the children were very concentrated and almost still. Changes resulting from possible head displacements within one sound were below perception (less than 1 dB) and in the case of successive sounds they were smaller than those resulting from voice stabilization (not exceeding 2 dB). Chosen test music material, according to instructions given to all persons individually, was to be sung freely "*mf*". Older children and students knew terms regarding dynamics; it was necessary to explain them to younger children in school language they understood. When it was noticed that a child was tense or his or her voice intensity was affected by the atmosphere in the damped booth, the teacher who knew the child's abilities in natural circumstances stopped the session and recording was repeated.

The sounds were recorded using an MCO 30 capacitance microphone, set in front of the singer, at a distance of 30 cm, and a MP 223 tape recorder. The source of standard sounds was a piano tuned before all sessions to an accuracy of 1 Hz. Frequency variations within one sound were in a 12-ct interval, i.e. within $+/-3$ Hz at a frequency of 440 Hz.

The range of test sound material was selected according to the abilities of the age groups, considering the scale range of individual children's voices and the programme recommendations for music classes in primary schools. For children's voices intoned sounds were from *a* (220 Hz) to e^2 (659.3 Hz); for adolescent voices, from *c* (130.8 Hz) to f^2 (698.5 Hz).

The number of sounds intoned by one voice was not the same, since the voices were untrained and, as it was already mentioned, could not always carry out the whole pitch scale.

Isolated sounds of the vowel "*a*" were intoned. All sounds were repeated five times.

The whole test material recorded underwent subjective auditory evaluation, called auditory evaluation below, and intonographic analysis was performed on the deep structure of the fundamental component using instrumentation adapted for music purposes, consisting of an intonographic set [11] and

a MERA 304 minicomputer (Fig. 1). Analog plotting (Fig. 2), being little accurate, was used only for evaluating the sound amplitude level and the signal to noise ratio. The error involved in frequency plotting depended on this ratio. Digital plotting was performed only for those sounds whose amplitude level exceeded 65 dB. A linear scale of the amplitude level (*AO*) was used with ac-

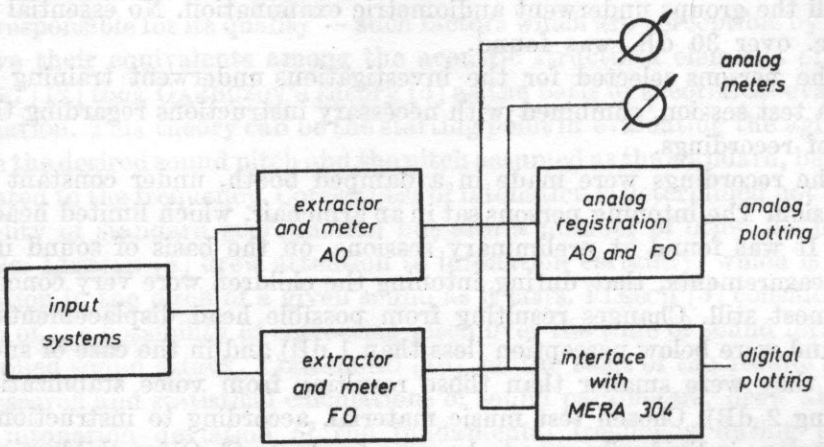

Fig. 1. A functional diagram of the intonograph [11]

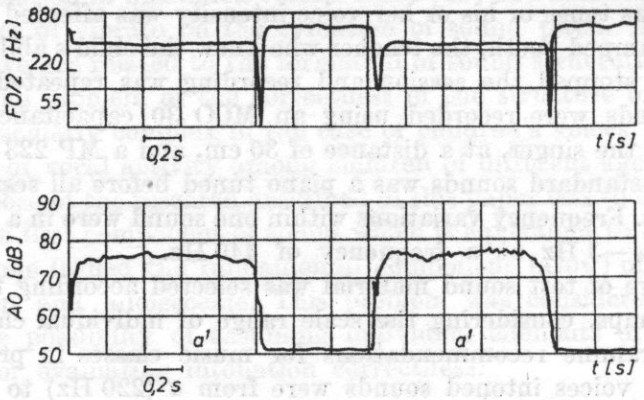

Fig. 2. An example of analog plotting (child 1/9, sound c^1)

curacy up to 1 dB over the range 50 dB to 90 dB and a logarithmic frequency scale (*FO*) from 85 Hz to 880 Hz. The frequency plotting density depended on the sampling frequency; the error in the plotting, on the signal to noise ratio. Intonographic plotting was made with constant time quantization at every 12.5 ms, providing the possibility of differentiating frequency in 12-ct zones for sounds of the little octave and half of the once-accented octave. Accomplishing such accuracy for higher sounds required their transposition by one octave lower. This made it possible to localize intonation deviations of

frequency with respect to the frequency of the sounds on a 12-tone scale in a regularly tempered system, in intervals of 12, 25, 50 and 75 ct for most of the sounds investigated. In a few cases of the twice-accented octave, where two adjacent intonation zones merged in the same code gate, it was assumed that there was a greater deviation, i.e. one less convenient from the point of view of intonation correctness.

Intonograms underwent statistical elaboration by calculating the mean, median and modal values, the standard deviation and one normalized for all sounds intoned individually. The correctness of taking for further elaboration one of the first three indexes was discussed. The following scale was assumed in evaluating the intonation deviations from the standard frequency: up to 12 ct – intonation without error, the deviation being within the Garbuzov zone for the prime; 25 ct – intonation within norm, this being the optimum zone of interval perception by everage gifted child; 50 ct – uncertain intonation; 75 ct – erroneous intonation; above 75 ct – completely wrong, the sound entering the zone of the solfeggio error.

3. Auditory evaluation

In order to confirm to what extent the properties of intoned sounds as given in the literature can constitute distinct, specific objects of evaluation based on a subjective sensation of intonation correctness, auditory evaluation of the sounds recorded was carried out. Three properties were considered: intonation clearness (*I*), understood as the agreement between the pitch of the sound monitored and the pitch recommended for intoning, i.e. the pitch of a piano sound; certainty of sound attack (*At*) and pitch stabilization (*St*) within one single sound.

These properties were selected as a result of a discussion of the evaluating group during preliminary monitoring training sessions. This group consisted of five persons, representatives of such specializations as vocalism education, secondary school music education, ear training, education of teachers for initial teaching of music and acoustics. The whole group had participated in monitoring sessions related to research for five years. At the preliminary sessions, the evaluation scale was also established. A four-point scale was assumed (3 points – no error, 2 – almost good, 1 – erroneous, 0 – quite wrong, solfeggio error). Attempts to introduce a wider scale led to completely diverging results in the evaluating group. These differences distinctly decreased with the point system assumed. E.g. full agreement in the evaluation of intonation clearness of sounds intoned by female voices was achieved in 17 per cent, only in the case of correct productions (3 points). In turn, in evaluating the sound attack in girls' voices, full agreement was achieved in 18 per cent only for the lowest marks (0 points).

The agreement of evaluations for particular properties is shown in Fig. 3 and, divided into female and male voices, in Table 1. The evaluations were classified as follows: 4 — all the same, 3 — one different by 1 point, 2 — 2-3 grouping with 1 — point difference or 1+4 grouping with greater difference,

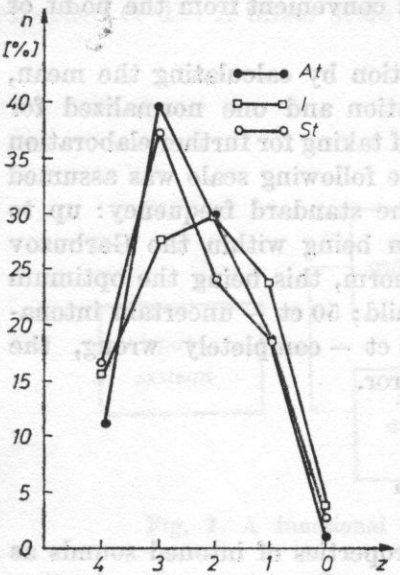

Fig. 3. The degree of agreement in auditory evaluation (z): correctness of pitch attack (At), intonation clearness (I) and pitch stabilization (St)

Table 1. The agreement in auditory evaluation

Voices	Total number of sounds evaluated	Agreement: 4 full	3 good	2 satisfactory	1 unsatisfactory	0 none
		[%]				
A. intonation clearness						
boys	98	19	19	24	32	6
girls	112	19	31	19	27	4
males	69	7	22	49	20	2
females	97	17	35	36	11	1
B. pitch attack						
boys	93	2	36	28	32	2
girls	112	18	36	27	18	1
males	65	11	48	23	18	0
females	82	11	45	35	9	0
C. pitch stabilization						
boys	91	14	36	21	28	1
girls	145	12	33	26	23	6
males	89	26	34	28	12	0
females	117	20	44	20	14	2

1 — evaluation differentiation by 2 points, 0 — evaluations from the highest (3) to the lowest (0) number of points. The greatest differences occurred in evaluating intonation clearness. A detailed analysis of this state of things is clearly beyond the scope of the present paper; it can only be mentioned that the results achieved previously [6] have been confirmed. This indicates the necessity of supporting auditory evaluation of intonation correctness with objectivizing methods, providing full control and also helpful in ear training.

4. Measured and calculated results

a. Duration and formation of the fundamental component

The duration of the fundamental component depends on the ability of sustaining a sound effortlessly in one breath. It was calculated from digital plotting of the amplitude level, considering the whole behaviour of the fundamental component from its initial excitation to the decay of the amplitude level to the noise level. The results were given in the form of histograms, with data grouped with an accuracy of 0.5 s. With children's voices this duration acheived its maximum value (and only in few cases) of about 1.5 s (Fig. 4). Sounds

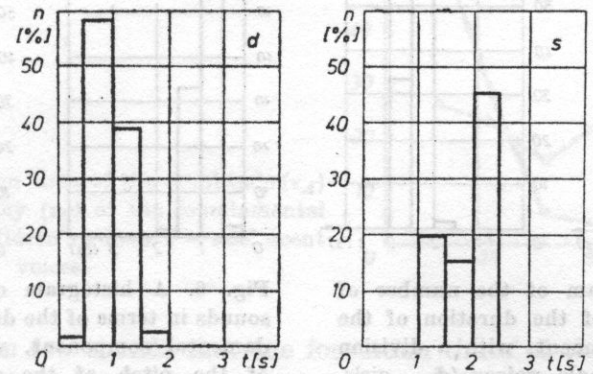

Fig. 4. A histogram of the number of sounds in terms of the duration of the fundamental component in the groups of children's (*d*) and adolescent (*s*) voices
n — the percentage of the sounds investigated

were most frequently kept in one breath for 0.5 to 1.0 s. This is an order of magnitude corresponding to the psychological present. According to Bielawski [2], the centre of the psychological present corresponds to 659 ms. The doubt arises as to whether over such a short time as the duration of the stabilized state of a sound intoned by a child, the listener can carry out an immediate analysis of pitch changes within the sound, resulting from frequency variation, and necessary in evaluating the stabilization. In teaching, this evaluation is most frequently performed by a person without acoustically trained analytic abilities.

Adult persons, without professional vocal training, tend to keep a sound in one breath for 2.0 to 2.5 s. With female voices the duration of the fundamental component is longer than with male ones (Fig. 5). It is therefore possible to assume an attitude towards the stabilization state of a sound while listening

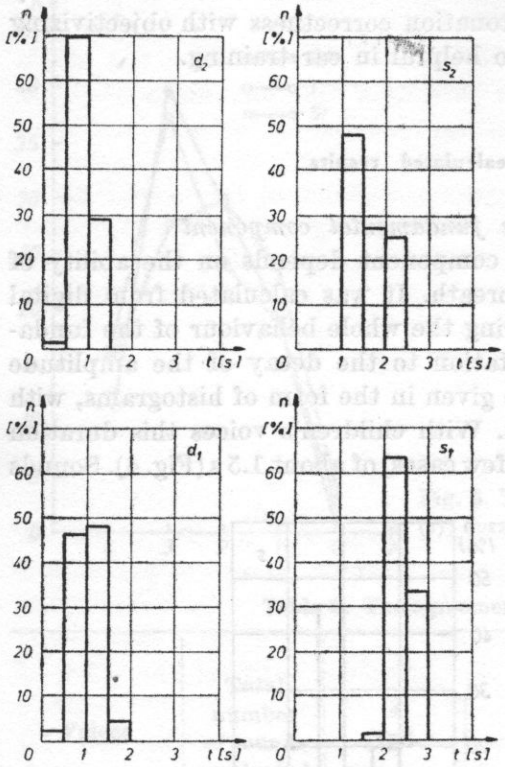

Fig. 5. A histogram of the number of sounds in terms of the duration of the fundamental component, with a division into female and male voices (d_1 — girls, d_2 — boys, s_1 — female, s_2 — male)

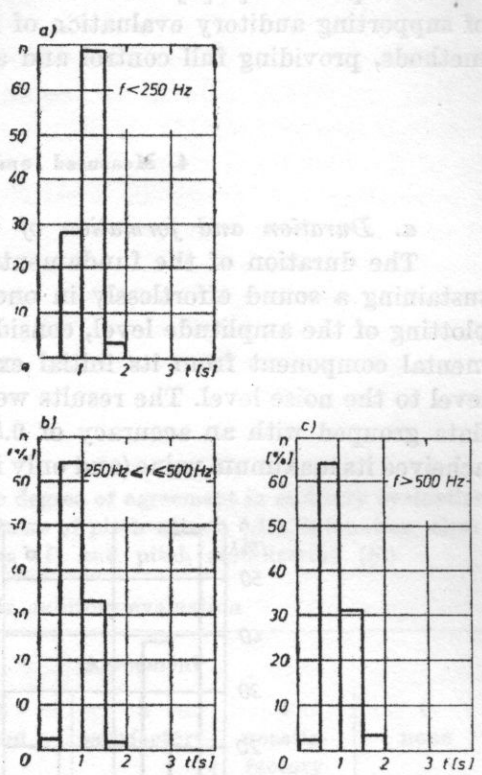

Fig. 6. A histogram of the number of sounds in terms of the duration of the fundamental component, with consideration of the pitch of the sounds (children's voices)

to it, which provides the basis for taking the frequency stabilization within a sound as one of criteria of evaluation of intonation correctness.

Adolescent voices were found to have greater ability to sustain in one breath higher sounds rather than lower ones. Children's voices did not show any distinct dependence of the duration of the fundamental component on the pitch of intoned sounds (Fig. 6).

Children attack sounds with great determination. The time necessary for the fundamental component frequency to stabilize is very short. In most cases the time does not exceed 37.5 ms, with the majority of results coinciding with 25.0 ms (Fig. 7). Over the sound attack interval in the behaviour of the

amplitude and frequency there sometimes occur variations which make it difficult to distinguish the moment when the stabilized state begins. Such "uncertain" intervals were included in the attack time. The formation times of both the frequency and the amplitude level above 50 ms are more often characteristic of adult (*s*) than children's (*d*) voices.

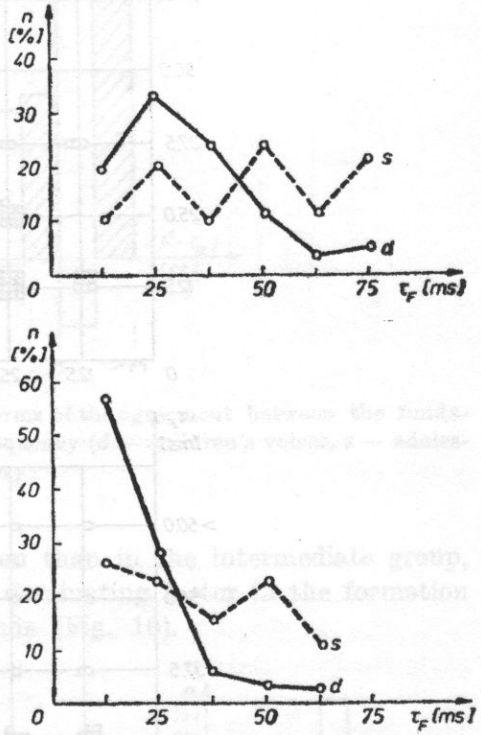

Fig. 7. The formation time of the amplitude (τ_A) and of the frequency (τ_F) of the foundamental component (*d* — children's voices, *s* — adolescent voices)

It is only in few sounds that the formation times of the frequency (τ_F) and of the amplitude level increase (τ_A) are equal (Fig. 8).

b. Fundamental component frequency vs nominal standard frequency

In order to determine the agreement between the fundamental component frequency and the nominal standard frequency of intoned sounds, the mean, median and modal values were calculated. These indexes were determined with reference to a section of the fundamental component indicating the properties of pitch stabilization or stabilization of pitch variation form, not shorter than 0.5 s. In about 90 per cent of analysed sounds these three indexes fell within the same interval of intonation accuracy. With large frequency scatter the modal value was not very distinct. In further calculations its mean value ($\overline{F}$) was taken as the frequency index.

The difference between the mean frequency ($\bar{F}$) and the nominal standard frequency (F_M) was assumed to be the measure of intonation deviation. The fundamental component frequency was found to decrease only in 1 per cent of sound in the group of adolescent voices and in 16 per cent in the

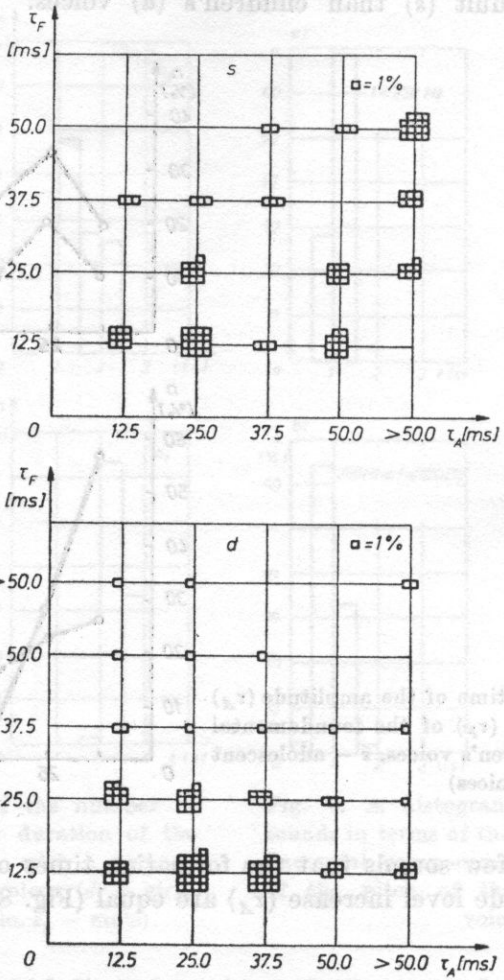

Fig. 8. The mutual relation between the formation time of the amplitude (τ_A) and that of the frequency (τ_F) of the fundamental component (*d* — children's voices, *s* — adolescent voices)

group of children's voices. In the other voices there was a distinct tendency towards an increase in the fundamental component frequency (Fig. 9).

Subjective evaluations of the intonation clearness appeared to be very lenient compared to the measurement results. Of 376 sounds evaluated, 226 were evaluated at 2 and 3 points. As it was already mentioned, there was, however, no full agreement in the evaluating group. It can be expected that apart from

subjective pitch sensation, complex factors played their role in this.

As the age of children's groups tested increases, the distribution of intonation deviation changes. Large deviations are more frequently found in the

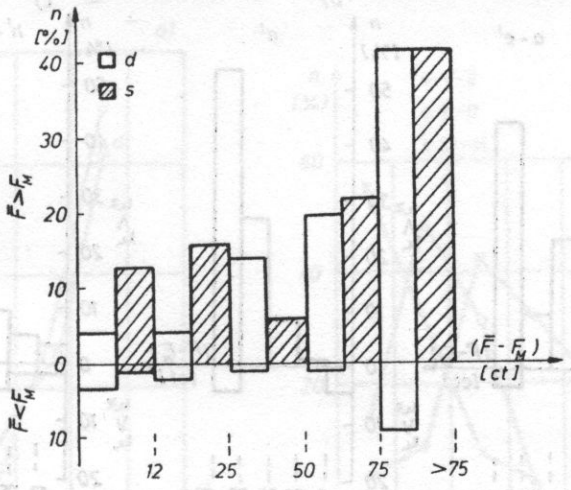

Fig. 9. A histogram of the number of sounds in terms of the agreement between the fundamental component frequency and the standard frequency (*d* — children's voices, *s* — adolescent voices)

groups of the youngest and eldest children than in the intermediate group, indicating that music training is not the dominating factor in the formation of the deep frequency structure of sounds (Fig. 10).

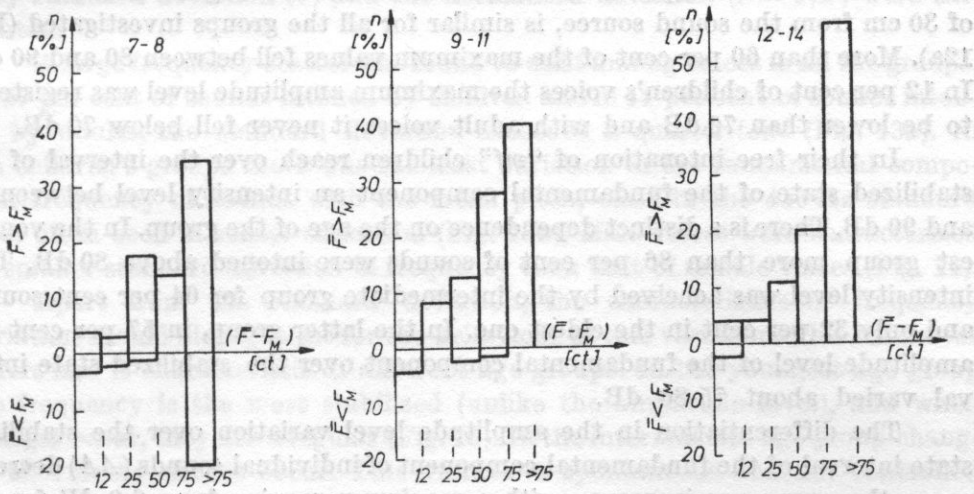

Fig. 10. A histogram of the number of sounds in terms of the agreement between the fundamental component frequency and the standard frequency, with consideration of the division of the intoning children into age groups

The intonation deviations were not found to depen don the pitch of intoned sounds (Fig. 11).

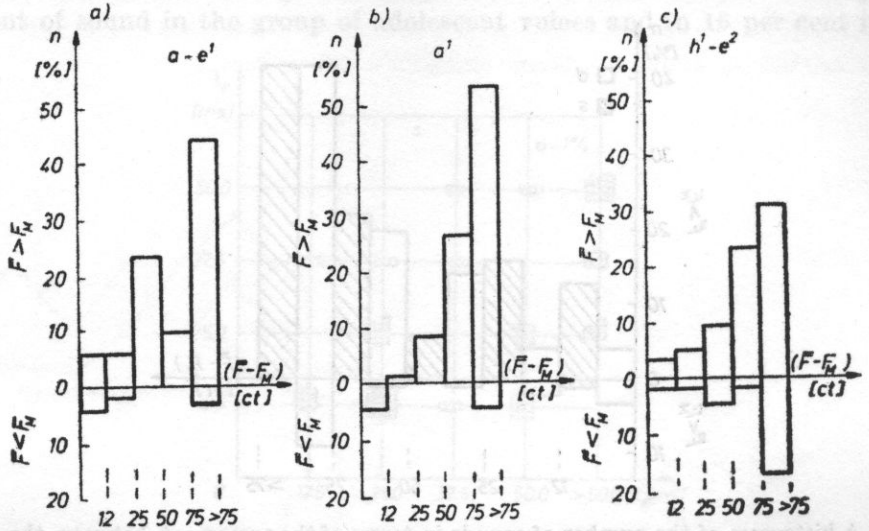

Fig. 11. A histogram of the number of sounds in terms of the agreement between the fundamental component frequency and the standard frequency, with consideration of the pitch of the sound intoned

c. Value and differentiation of the amplitude level

The distribution of the value of the amplitude level (A), characteristic of the fundamental component of the intoned sound "mf" registered at a distance of 30 cm from the sound source, is similar for all the groups investigated (Fig. 12a). More than 60 per cent of the maximum values fell between 80 and 90 dB. In 12 per cent of children's voices the maximum amplitude level was registered to be lower than 70 dB and with adult voices it never fell below 70 dB.

In their free intonation of "*mf*" children reach over the interval of the stabilized state of the fundamental component an intensity level between 55 and 90 dB. There is a distinct dependence on the age of the group. In the youngest group more than 86 per cent of sounds were intoned above 80 dB. This intensity level was acheived by the intermediate group for 64 per cent sounds and only 32 per cent in the eldest one. In the latter group, in 57 per cent the amplitude level of the fundamental component over the stabilized state interval varied about 75-80 dB.

The differentiation in the amplitude level variation over the stabilized state interval of the fundamental component of individual sounds (ΔA) decreases as the group age increases, with a maximum moving from 6-9 dB for the youngest group to 0-3 dB for the eldest (Fig. 12b).

In the voices of the adult group the amplitude level of individual sounds also varied. This variation over the stabilized interval of the fundamental component is mostly 3-4 dB for female voices and 6 dB for male ones.

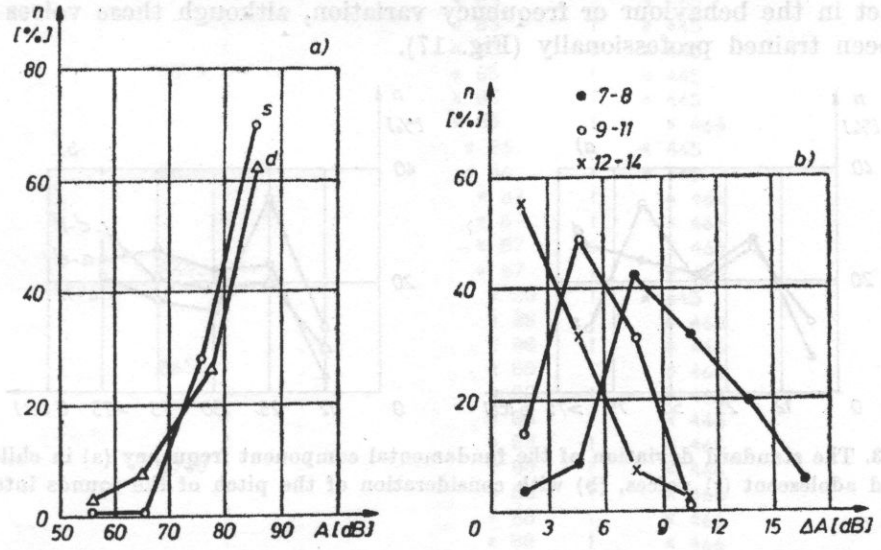

Fig. 12. The maximum value (*a*) and differentiation (*b*) of the amplitude level of the fundamental component of the freely intoned sounds "*mf*" (*d* — children's voices, *s* — adolescent voices).

d. Variation in the fundamental component frequency

In order to gain information about the frequency variation within one sound over the stabilized interval of the fundamental component, the frequency standard deviation (σ) and the normalized deviation ($v = \sigma/\overline{F}$) were calculated.

A large frequency scatter was found to exist among voices in all the groups. In 47 per cent of sounds intoned by children and in 44 per cent of sounds intoned by adults, the standard deviation exceeded a quarter-tone (Fig. 13a). In the children's groups there was the least variation in the fundamental component frequency of sounds with the mean pitch, close to the 440 Hz standard most often used in school education (Fig. 13b). Male voices were characterized by smaller standard deviation in frequency than that of female voices (Fig. 14).

Apart from the standard deviation, the characteristics of frequency variation should also account for the behaviour of this variation. This behaviour differs and is characteristic of different age groups. In the youngest age group the frequency is the most stabilized (unlike the amplitude level), and when changes occur, they are irregular (Fig. 15). In the intermediate age group changes of vibrato nature occur. This vibrato is spontaneous and not controlled by the intoning person [17]; it has no artistic significance. With the usual relatively short time over which a child keeps a sound in one breath, he or

she is unable to form a stabilized vibrated interval. With the eldest children, in all the sounds there occurs vibration of the fundamental component frequency (Fig. 16). In adult voices, particularly female ones, the vibrato form is quite distinct in the behaviour or frequency variation, although these voices have not been trained professionally (Fig. 17).

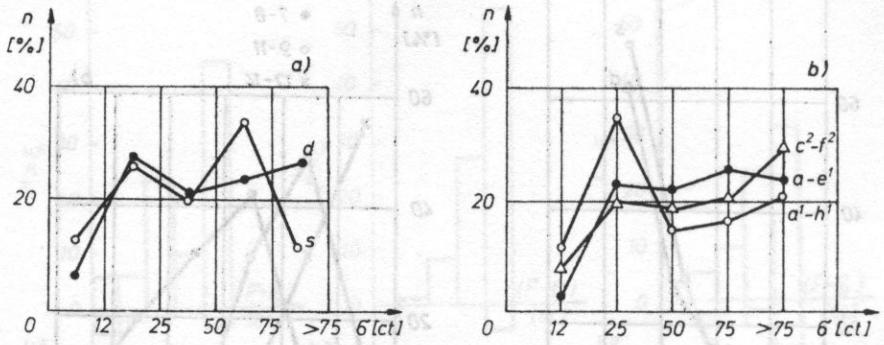

Fig. 13. The standard deviation of the fundamental component frequency (a) in children's (*d*) and adolescent (*s*) voices, (b) with consideration of the pitch of the sounds intoned

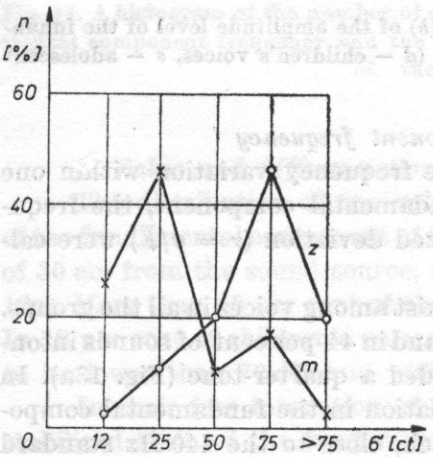

Fig. 14. The standard deviation of the fundamental component frequency in male (*m*) and female (*z*) adolescent voices

The frequency intonation deviation, measured by the normalised deviation (ν), usually takes values from 2 to 8 per cent (Fig. 18a).

The least regular distribution is characteristic of the lowest sounds (Fig. 18b). Low sounds are often difficult for the youngest children to intone. The distribution of the normalised deviation in children's voices is similar to those of the youngest and eldest groups of children (Fig. 19a), but its causes are different for the two groups. In the group of children 7-8 years old the great frequency variation within the stabilized state of the first fundamental component of a sound results from their inability to intone, i.e. from the uncertainty of

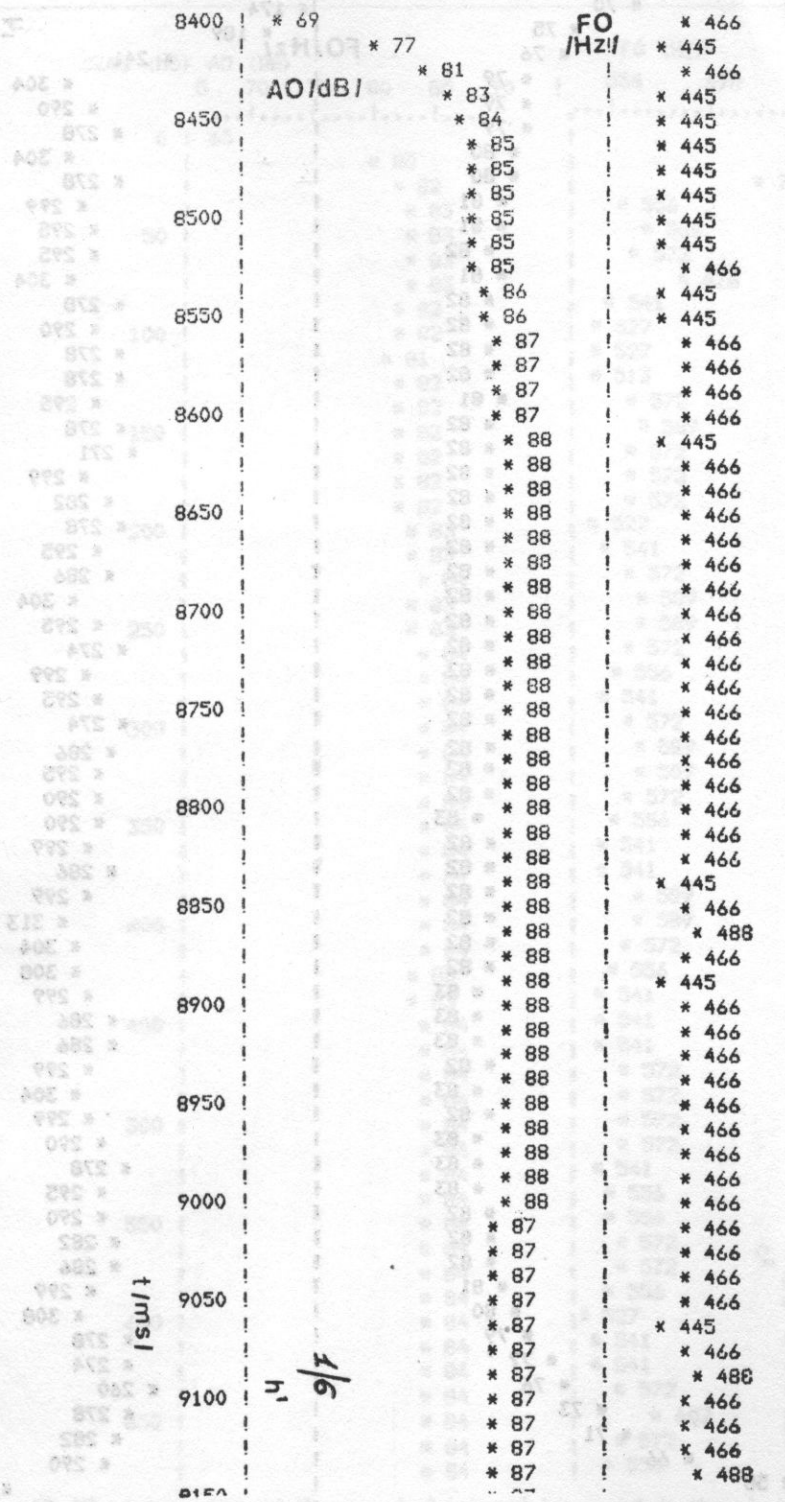

Fig. 15. The intonogram of the sound h^1 intoned by an 8-year-old child

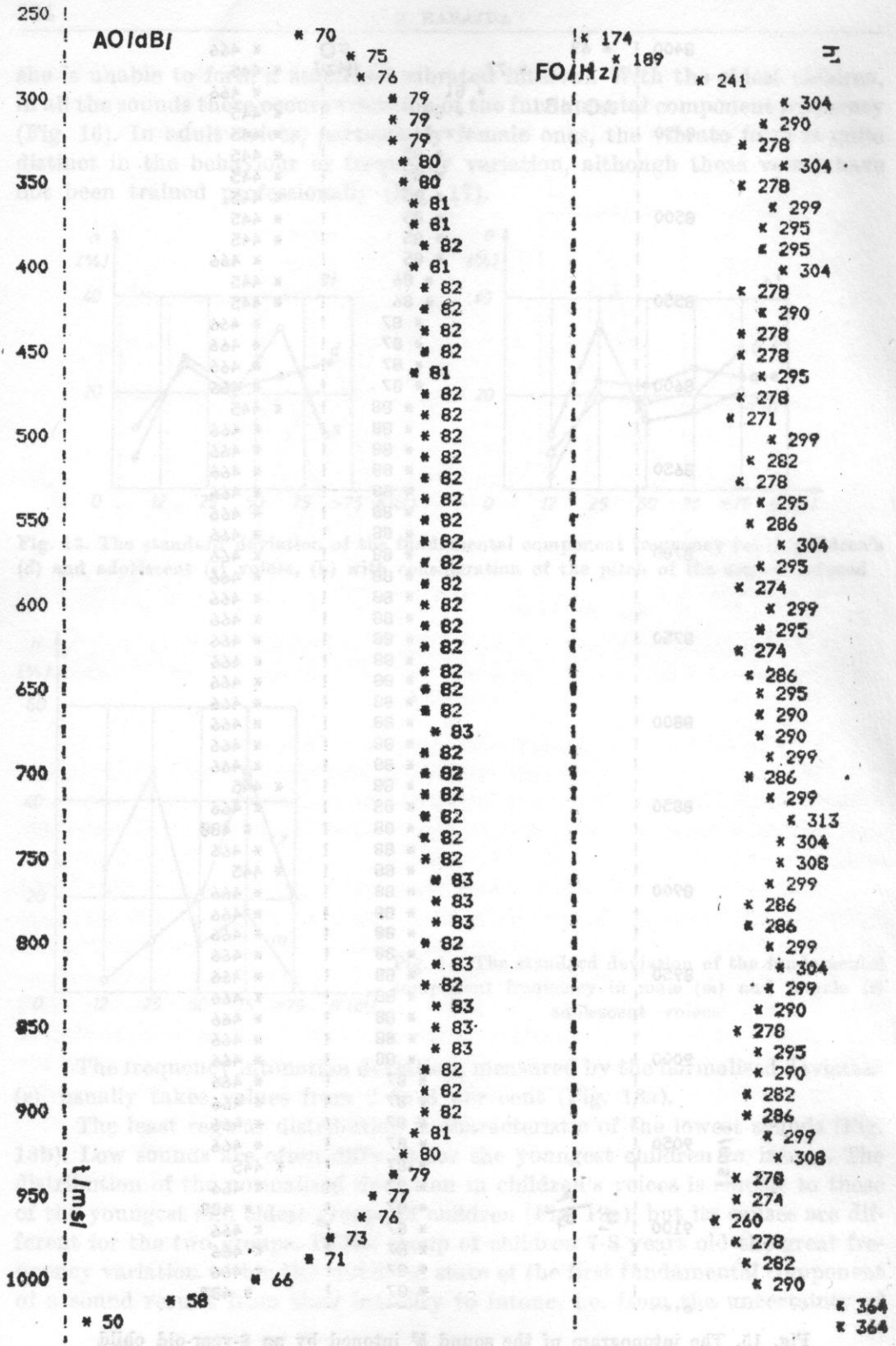

Fig. 16. The intonogram of the sound A[1] intoned by a 13-year-old child

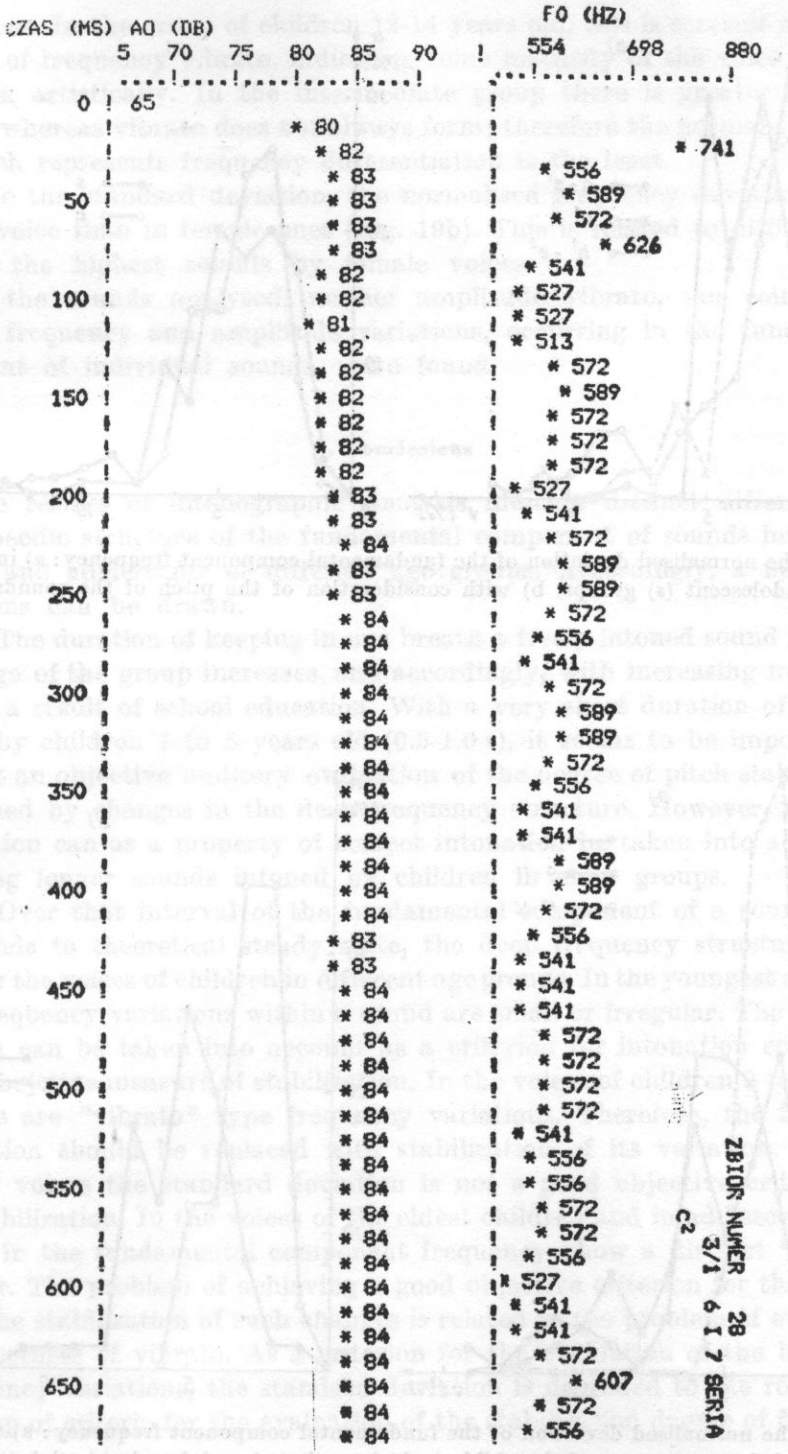

Fig. 17. The intonogram of the sound c^2 intoned by an adult (female adolescent voice)

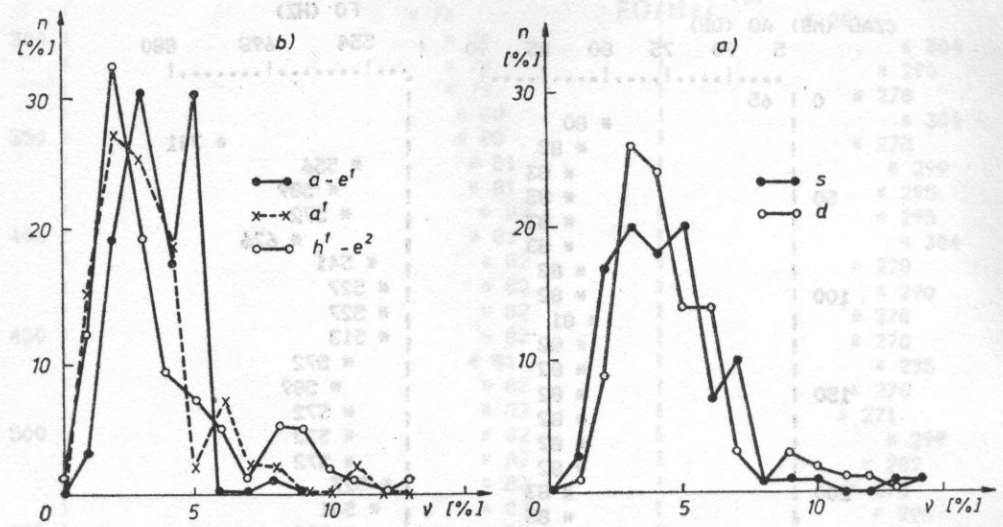

Fig. 18. The normalised deviation of the fundamental component frequency: a) in children's (*d*) and adolescent (*s*) groups, b) with consideration of the pitch of the sounds intoned

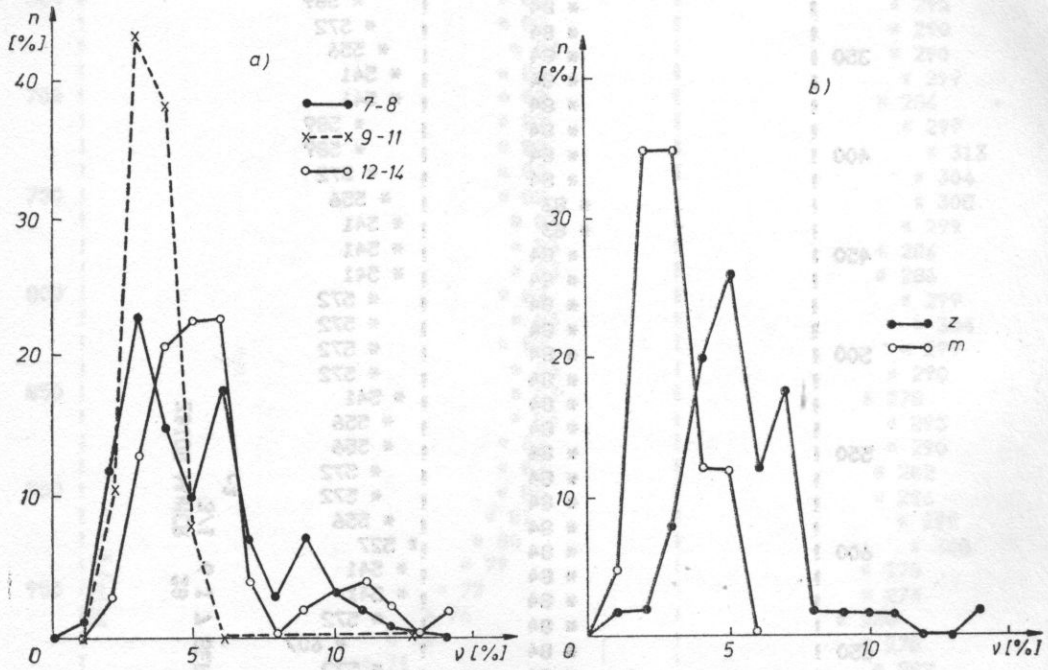

Fig. 19. The normalised deviation of the fundamental component frequency: a) with consideration of the age groups of the children, b) in male (*m*) and female (*z*) adolescent voices

their voices. In the group of children 12-14 years old, this is a result of the occurrence of frequency vibrato, indicating some maturity of the voice to shape intonation artistically. In the intermediate group there is greater certainty of voice, whereas vibrato does not always form; therefore the normalised deviation which represents frequency differentiation is the least.

Like the standard deviation, the normalised frequency deviation is less in male voice than in female ones (Fig. 19b). This is related to difficulties in intoning the highest sounds by female voices.

In the sounds analysed, neither amplitude vibrato, nor coincidences between frequency and amplitude variations, occurring in the fundamental component of individual sounds, were found.

5. Conclusions

The results of intonographic analysis indicate distinct differentiation in the specific structure of the fundamental component of sounds intoned by children and adolescents of different age groups. Accordingly, a number of conclusions can be drawn.

1. The duration of keeping in one breath a freely intoned sound increases as the age of the group increases, and accordingly, with increasing music abilities, as a result of school education. With a very short duration of a sound intoned by children 7 to 8 years old (0.5-1.0 s), it seems to be impossible to carry out an objective auditory evaluation of the degree of pitch stabilization, conditioned by changes in the deep frequency structure. However, the pitch stabilization can as a property of correct intonation be taken into account in evaluating longer sounds intoned by children in elder groups.

2. Over that interval of the fundamental component of a sound which corresponds to theoretical steady state, the deep frequency structure is different for the voices of children in different age groups. In the youngest children's voices frequency variations within a sound are small or irregular. The standard deviation can be taken into account as a criterion for intonation correctness and an obejctive measure of stabilization. In the voices of children 9 to 11 years old there are "vibrato" type frequency variations. Therefore, the frequency stabilization should be replaced with stabilization of its variation. For this group of voices the standard deviation is not a good objective criterion for pitch stabilization. In the voices of the eldest children and in adolescent voices changes in the fundamental component frequency show a distinct "vibrato" character. The problem of achieving a good objective criterion for the evaluation of the stabilization of such changes is related to the problem of evaluating the correctness of vibrato. As a criterion for the evaluation of the behaviour of frequency variations, the standard deviation is degraded to the role of one of a group of criteria for the evaluation of the stabilization degree of frequency behaviour.

3. In the voices investigated no "vibrato" type changes were found in the behaviour of the amplitude level, nor, as BJÖRKLUND [1] suggests, any changes in the regularity of the variation of its level.

4. The desired fundamental component frequency of a sound and its highest amplitude level are not achieved in the same time. The time of the frequency attack is usually shorter than the time of amplitude level stabilization. In children's voices, irrespective of a child's age, it is very short. In adolescent voices the time of the frequency attack is longer than in children's voices, but not so long as to permit the listener to grasp with his ear differences over that interval and to be assumed as the criterion for intonation correctness. Therefore, the conception mentioned by LESMAN [8], regarding bow instruments, that intonation should be corrected over the interval of the sound attack, does not seem to be useful in evaluating the correctness of attacking the pitch of vocal sounds.

However, the stabilization time of the amplitude level of the fundamental component, which is longer than the pitch attack time, justifies the taking into account of this parameter as one of criteria potentially useful in evaluating intonation correctness.

5. Calculations of the intonation deviation from the differences between the mean fundamental component frequency and the nominal standard frequency have shown that the frequency tends to increase in all the groups investigated, except the youngest. In 60 per cent of subjective auditory evaluations sounds of increased fundamental component frequency were estimated as completely or almost correct in terms of intonation clearness.

References

[1] A. BJÖRKLUND, *Analyses of soprano voices*, J. Acoust. Soc. Am., 5, 21-25 (1961).

[2] L. BIELAWSKI, *Zonal theory of time* (in Polish), PWM, Cracow 1976.

[3] C. FLESCH, *Art of violin play* (in Polish), PWM, Cracow 1960.

[4] H. FUJISAKI, *Dynamic characteristics of voice fundamental frequency in speech and singing*, Proc. F.A.S.E. 1981, II, 57-70.

[5] N. A. GARBUZOV, *Zonnaya priroda zvukovysotnogo swukha* (in Russian), AN ZSRR, Moscow 1948.

[6] H. HARAJDA, R. HARAJDA, *Problems of music education technology* (in Polish), Neodidagmata, XIII, 215-221 1981.

[7] H. HARAJDA, W. MIKIEL, P. ŻARNECKI, *Le son vocal intonné sur la voyele "a" dans l'image intonographique*, Fortschritte der Akustic, FASE/DAGA 83, Göttingen, 895-898, 1982.

[8] I. LESMAN, *Directions in violinist's development. Nature and development of clear intonation* (in Polish), Tyton, Leningrad 1934.

[9] S. M. MAYKAPAR, *Musical hearing its significance, nature, properties and the method of correct development* (in Polish), Muzgiz, Petrograd 1915.

[10] W. MIKIEL, P. ŻARNECKI, *Acoustic parameters of speech signals in children* (in Polish), Proc. XXIV Open Seminar on Acoustics 1977, 1, 124-127.

[11] W. MIKIEL, R. GUBRYNOWICZ, W. HAGMAJER, *Intonograph – a system for the measurement and visualization of speech intensity and melody* (in Polish), Proc. XXIV Open Seminar on Acoustics 1977, **1**, 120-123.

[12] K. MOSTAS, *Intonation in violin play* (in Polish), PWM, Cracow 1958.

[13] Yu. RAGS, *Vibrato i vospriyatie vysoty* (in Russian), Prim Akust. Metodov Issledovanya v Muzykoznanii, Izd. Muzyka, Moscow 1964.

[14] A. RAKOWSKI, *Categorical perception of sound pitch in music* (in Polish), PWSM, Warsaw 1978.

[15] J. SEYMOUR, *Acoustic analyses of singing voices*, Acustica, **27**, 4 (1972).

[16] P. TJERNLUND, J. SUNDBERG, F. FRANSSON, *Grundfrequenzmessungen an schwedischen Kernsplatfloten*, Musikhistoriskamuseet, Stockholm 1972.

[17] T. WROŃSKI, *Problems of violin play. Intonation* (in Polish), PWM, Cracow 1951.

[18] T. ZALESKI, *Vocal apparatus and vocal technique* (in Polish), COPSA, Warsaw 1962, p. 61.

Received on 18 November, 1982

ARCHIVES OF ACOUSTICS
8, 4, 293-316 (1983)

EXPERIMENTAL METHODS OF IDENTIFYING SOUND SOURCES ON A MACHINE

MALCOLM J. CROCKER

Ray W. Herrick Laboratories, School of Mechanical Engineering, Purdue University
(West Lafayette Indiana 47907, USA)

There are many existing methods to identify noise sources and paths and some newer methods have also been recently developed. Several existing techniques have been used to identify noise sources on machines for many years. None are completely satisfactory. They are usually inaccurate, expensive, time consuming and often need special acoustic facilities. The most commonly used technique is perhaps the selective-wrapping or lead-wrapping approach. Recently, fast Fourier transform (*FFT*) minicomputers have become widely available and theory has been published for the calculation of acoustic intensity from two simultaneously measured signals. Two new techniques have been investigated by a number of research workers. These two techniques are: the surface intensity approach (microphone-accelerometer) and the acoustic intensity approach (two-microphone). These two new techniques can be used to study sound sources and sound paths and will be discussed in this paper in some detail. The paper begins with a brief review of some of the earlier methods, continues with a description of other methods of noise source identification and concludes with a discussion of the newer intensity and coherence techniques to identify machinery noise sources and paths.

1. Introduction

The use of road vehicles has now become so widespread in industrialized countries that their gaseous emissions have become a health hazard and their noise unbearable for a large fraction of the population in many large cities [1, 2]. In addition, the noise in some industrial plants is so intense that large numbers of workers in many countries have suffered permanent hearing loss.

The reduction of vehicle and machinery noise has become a priority item for many governments and several countries have produced noise regulations for industrial machinery and vehicles. In order to reduce machinery and vehicle noise it is important first to gain some knowledge of noise sources. Once this

knowledge is obtained, then it may be possible to make engineering changes to reduce the strength of different sources or interfere with the paths of noise propagation by use of absorption, enclosure or vibration-isolation.

In most such machinery noise control problems, a knowledge of the dominant noise sources in order of importance is very desirable so that modifications can be made in a logical way. In a complicated machine, such noise source information is often difficult to obtain and many noise reduction attempts are made based on inadequate data so that frequently expensive or inefficient noise reduction methods are employed. Information on noise paths is also needed so that the most suitable path noise control techniques mentioned above can be attempted, and the whole noise control solution optimized.

2. Review of classical methods of identifying sources

The sound field produced by a noise source is normally quite complicated and several of its properties are of interest. These include: variation of the sound pressure magnitude and sound power with frequency, directivity of the sound field and variation of sound pressure level with distance from the source and with time.

Several noise source identification methods have been used on machinery for a long time. A brief review of these methods follows.

2.1 *Subjective assessment*

With practice the ear can often distinguish between sounds more accurately than can sophisticated measuring equipment. The ear should always be used as the first noise source identification approach. However, it does not give quantitative results.

2.2 Selective operation

Selective operation is also a useful approach [3]. Sometimes with a complicated machine it is possible to operate the machine with some parts disconnected and simultaneously to measure the noise of the machine. Providing such a procedure does not alter the operation of the machine significantly, it can often be used to indicate the contribution of the different parts to the complete machine noise when all the parts are operating simultaneously. However, great care must be used with this approach.

2.3 Selective wrapping

Selective wrapping has often been used with vehicles and engines. It is often used in conjunction with selective operation. Fig. 1 shows the contributions of different sources on an International Harvester truck, during a drive-by test, which were obtained by a combination of the selective operation techniques [4]. With the truck, the engine was wrapped, the exhaust suppressed with an oversize muffler and the cooling fan removed. The selective wrapping

technique is also often used on engines. Usually a heat resisting, absorbing material is used, enclosed with a massive material such as lead. However, the selective wrapping technique is tedious and time consuming and there has been a search for quicker, more convenient methods of source identification.

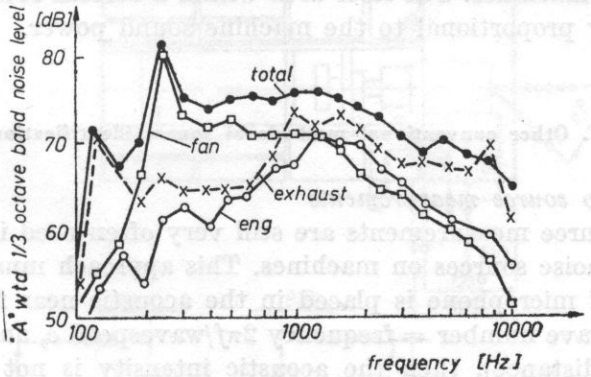

Fig. 1a. One-third octave analysis of truck total and other noise

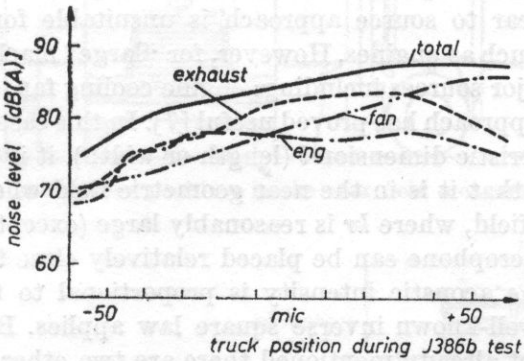

Fig. 1b. The fan noise contributes most to total noise

2.4 Frequency analysis

Frequency analysis of sound power is often required to describe a noise source properly. Narrow band information used to be obtained using analog equipment. Such information can be now obtained more quickly using fast Fourier transform (*FFT*) digital computers. In some cases a narrow band frequency analysis can also be used to identify pure tone sources of sound. Engine-firing, fan-blade-passage, and gear-meshing frequencies can all be calculated and identified. As the vehicle (or engine) speed is changed, such frequencies will normally change as predicted. If peaks in the frequency spectrum do not change with speed this suggests that they are caused by resonance frequencies o efficient transmission or radiation at such frequencies [3, 5].

2.5 Mapping

Mapping of contours of equal sound pressure level around a source is a useful approximate guide to major sound sources on a large fixed machine [6]. This method can also be used to give a rough estimate of the sound power emitted by different machines. The floor area within a certain sound level contour is approximately proportional to the machine sound power.

3. Other conventional methods of source identification

3.1 Near to source measurements

Near to source measurements are still very often used in an attempt to identify major noise sources on machines. This approach must be used with extreme care. If microphone is placed in the acoustic near field where kr is small (k is the wave number = frequency $2\pi f$/wavespeed c, and r is the source to microphone distance), then the acoustic intensity is not proportional to sound pressure squared and this gives misleading results. This is particularly true at low frequency. The acoustic near field is reactive; the sound pressure is almost completely out-of-phase with the acoustic particle velocity.

Thus, this near to source approach is unsuitable for use on relatively "small" machines such as engines. However, for "large" machines such as vehicles with several major sources including: engine cooling fan, exhaust, inlet, etc., the near to source approach has proved useful [7]. In this case where the machine is large, of characteristic dimension l (length or width), it is possible to position the microphone so that it is in the near geometric field where r/l is small, but in the far acoustic field, where kr is reasonably large (except at low frequency). In this case the microphone can be placed relatively close to each major noise source and now the acoustic intensity is proportional to the sound pressure squared and the well-known inverse square law applies. Besides the acoustic near to source effect already mentioned there are two other potential problems with this approach: *i*) source directivity and the need to use more than one microphone to describe a large noise source, *ii*) contamination of microphone signals placed near individual sources by sound from other stronger sources. Unfortunately, contamination cannot be reduced by placing the microphones closer to the sources because then the acoustic near field effect is increased. However, contamination from other strong sources can be allowed for by empirical correction using the inverse square law and the distance to the contaminating source.

Despite the various potential problems with the near to source method, WANG and CROCKER have used it quite successfully to identify the major noise sources on a large diesel engine truck [7]. By placing microphones near each major noise source (Fig. 2) and then extrapolating to a position 14.5 m from the truck (Fig. 4) good agreement could be obtained with earlier selective ope-

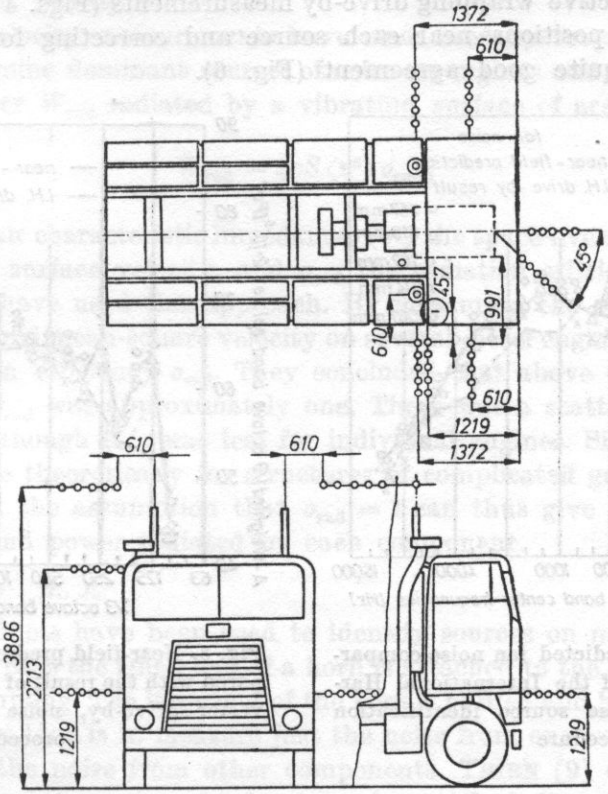

Fig. 2. Microphone positions in the near-field measurement

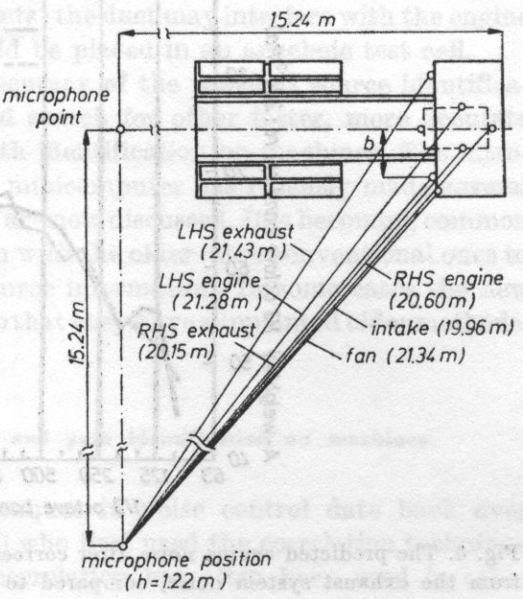

Fig. 3. The position of the track on the sound pad when the truck engine reached its governed speed of 2100 rpm with 6th gear in the International Harvester noise source identification test

ration and selective wrapping drive-by measurements (Figs. 4 and 5). Averaging over five positions near each source and correcting for contaminating sources gave quite good agreement (Fig. 6).

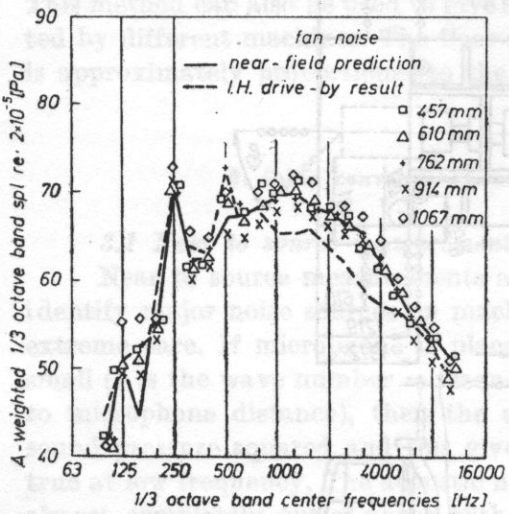

Fig. 4. Near-field predicted fan noise compared with the result of the International Harvester drive-by, noise source identification procedure

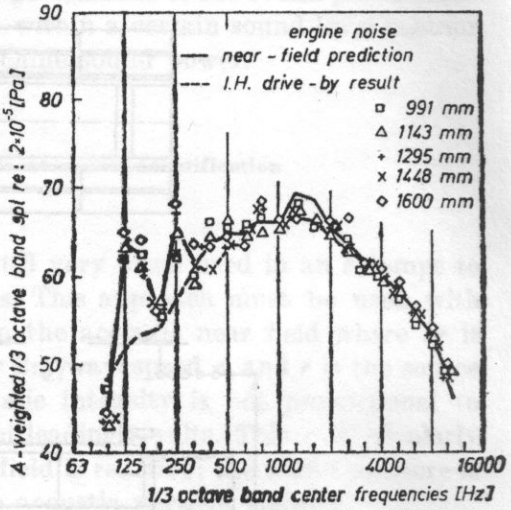

Fig. 5. Near-field predicted engine noise compared with the result of the International Harvester drive-by, noise source identification procedure

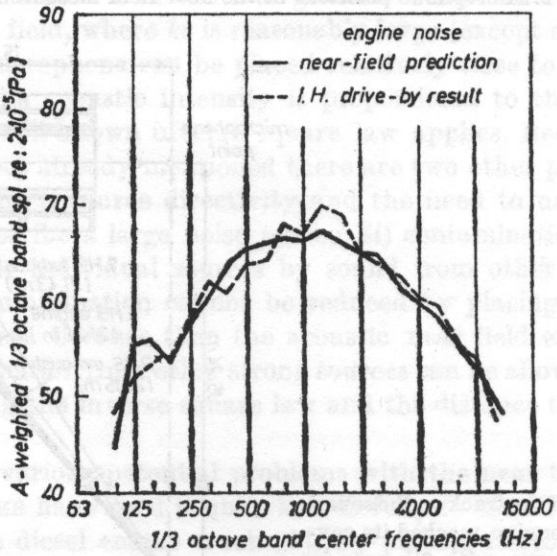

Fig. 6. The predicted engine noise after corrections are made to eliminate the contribution from the exhaust system noise, compared to the International Harvester drive-by result

3.2 Surface velocity

Surface velocity measurements have been used by several investigators to try to determine dominant sources of noise on engines and other machines. The sound power W_{rad} radiated by a vibrating surface of area S is given by

$$W_{rad} = \varrho c S \langle v^2 \rangle \sigma_{rad}, \tag{1}$$

where ϱc is the air characteristic impedance, $\langle v^2 \rangle$ the space-average of the mean-square normal surface velocity, and σ_{rad} the radiation efficiency. CHAN and ANDERTON [8] have used this approach. By measuring the sound power and the space-averaged mean-square velocity on several diesel engines they calculated the radiation efficiency σ_{rad}. They concluded that above 400 Hz for most diesel engines σ_{rad} was approximately one. There was a scatter of ± 6 dB in their results, although this was less for individual engines. Since σ_{rad} is difficult to calculate theoretically for structures of complicated geometry such as a diesel engine, the assumption that $\sigma_{rad} = 1$ can thus give an approximate idea of the sound power radiated by each component.

3.3 Acoustic ducts

Acoustic ducts have been used to identify sources on machines such as engines. In this case the small end of a horn is attached to the engine structure by a flexible coupling. The large end of the horn is baffled and has a microphone placed in it. The idea is to measure just the noise from one engine component and to isolate the noise from other components. THIEN [9] claims that this method is as accurate as the selective wrapping method. However, it should be noted that there are potential problems. Sealing the duct to the engine may be difficult with different size components; the duct may interfere with the engine radiation and ideally the engine should be placed in an anechoic test cell.

Problems with cost, time and accuracy of the previous source identification methods have led to a continued search for other faster, more accurate alternative methods of source and path identification on machines. The introduction of the fast Fourier transform minicomputer has recently made several of these reasonably successful and they are now discussed. It is becoming common to use the new techniques in conjuction with the older more conventional ones to give added confidence in the noise source information. In some cases the new techniques are sufficiently developed so that they have supplanted older methods.

4. Coherence technique of source and path identification on machines

Correlation and coherence techniques in noise control date back over twenty years to the work of GOFF [10] who first used the correlation technique to identify noise sources. Although correlation has often been used in other

applications it has not been widely used in noise source and path identification. One exception is the work of KUMAR and SRIVASTAVA who reported some success with this technique in identifying noise sources on diesel engines [11]. Since the ear acts as a frequency analyzer, the corresponding approach in the frequency domain (coherence) instead of the time domain is usually preferable. CROCKER and HAMILTON have recently reviewed the use of the coherence technique

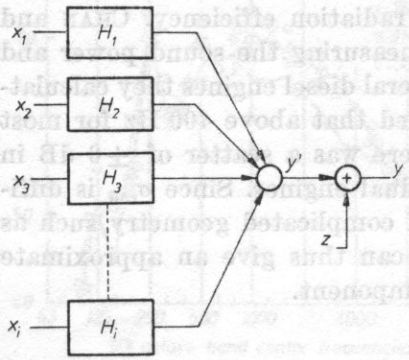

Fig. 7. A multiple input, single output system with uncorrelated noise at the output

in modelling diesel engine noise [5]. Such a coherence model can also be used in principle. Fig. 7 shows an idealized model of a multiple-input, single-output system. It can be shown [5] that the auto spectrum of the output noise S_{yy} is given by

$$S_{yy} = \sum_{i=1}^{N} \sum_{j=1}^{N} S_{ij} H_i H_j^* + S_{zz}, \tag{2}$$

where N is the number of inputs, S_{ij} are cross spectral densities between inputs, H_i are frequency responses and S_{zz} is the autospectral density of any uncorrelated noise z present at the output. Note that the S and H terms are frequency-dependent.

If there are N inputs, then there will be N equations,

$$S_{iy} = \sum_{j=1}^{N} H_j S_{ij}, \quad i = 1, 2, 3, \ldots, N. \tag{3}$$

The frequency responses $H_1, H_2, H_3, \ldots, H_N$ can be found by solving the set of N equations (3). The multiple coherence function $\overline{\gamma_{xy}^2}$ is defined to be

$$\overline{\gamma_{xy}^2} = S_{y'y'}/S_{yy}, \tag{4}$$

where $S_{y'y'}$ is the output noise coherent with all the inputs and is the first term on the right of equation (2);

$$S_{y'y'} = \sum_{i=1}^{N} \sum_{j=1}^{N} S_{ij} H_i H_j^* . \tag{5}$$

The multiple coherence function $\overline{\nu_{xy}^2}$ represents the fraction of the output which is coherent with all the inputs. From equations (2), (4) and (5)

$$\overline{\nu_{xy}^2} = 1 - (S_{zz}/S_{yy}). \tag{6}$$

The value of $\overline{\nu_{xy}^2}$ falls between 0 and 1.

CHUNG, SEYBERT, CROCKER and HAMILTON have used the coherence approach to model diesel engine noise [5, 12-14]. This approach appears to give useful information on a naturally aspirated diesel engine which is combustion-noise dominated and where the N inputs are $x_1 \ldots x_N$, the cylinder pressures measured by pressure transducers in each cylinder (see Fig. 7). In this case, H_i, the frequency response (transfer function between the ith cylinder and the far field microphone) can be calculated. Provided proper frequency averaging is performed, the difficulty of high coherence between the cylinder pressures can be overcome because the phasing between the cylinder pressures is exactly known [15]. In this case the quantity $S_{ii}|H_i|^2$ may be regarded as the far field output noise contribution by the ith cylinder. This may be useful noise source information for the engine designer.

HAYES, SEYBERT and HAMILTON in further research at Herrick Laboratories have extended this coherence approach to try to separate combustion noise from piston-impact noise in a running diesel engine [16].

WANG and CROCKER showed that the multiple coherence approach could be used successfully to separate the noise from sources in an idealized experiment such as one involving three loudspeakers, even if the source signals were quite coherent [17, 18]. However, when a similar procedure was used on the more complicated case of a truck which was modeled as a six input system (fan, engine, exhaust (s), inlet, transmission) the method gave disappointing results and the simpler near to source method appeared better [7, 17]. The partial coherence approach was also used in the idealized and truck experiments. It is believed that contamination between input signals and other computational difficulties may have been responsible for the failure of the coherence method of identifying truck noise sources.

Some workers have recently used the coherence approach with the simplifying assumption that all the sources are incoherent. In this case the cross spectral terms S_{ij} in equation (2) are zero and only the autospectral densities S_{ji} are retained. This simplified approach is sometimes known as the ordinary coherence function method. It has been applied with most success where the sources are definitely incoherent, e.g. where there are many independent machines [50].

5. Noise source and path identification using intensity technique

5.1 Intensity in a sound field

The intensity I is the net rate of flow of sound energy per unit area. The intensity I_r in the r direction is

$$I_r = \langle p u_r \rangle, \tag{7}$$

where p is the instantaneous sound pressure, u_r is the sound particle velocity in the r direction and $\langle\ \rangle$ denotes a time average. The sound power W radiated by a source can be obtained by integrating the component of the intensity, I_n, normal to any surface S enclosing the source,

$$W = \int_S I_n dS. \tag{8}$$

5.2 Noise source identification using the surface intensity technique

The surface intensity technique which uses an accelerometer mounted on a vibrating surface and a microphone located close to the accelerometer has been under development since about 1974. MACADAM described the use of this technique in the measurement of the sound power radiated from room surfaces in lightweight buildings [19, 20]. HODGSON also discussed this technique and its use on a large centrifugal chiller machine [21]. CZARNECKI *et al.* [22] successfully compared the sound power of a pure-tone excited, rigid, circular, baffled piston source obtained from surface intensity measurements, the conventional reverberation room method, as well as the free-field method and theory. BRITO investigated theoretically and experimentally the case of a vibrating rectangular flexible panel and obtained good agreement [23, 24]. KAEMMER and CROCKER [25, 26, 27] measured the sound power of a vibrating cylinder using the surface intensity method and compared it with the reverberation room method and theory. They obtained good results when they carefully accounted for phase shifts between the microphone and accelerometer signals.

In the case of surface intensity measurements, the particle velocity u_n normal to the vibrating surface area S can be found by integrating the signal from an accelerometer. The pressure p can be measured by a microphone close to the accelerometer. If the instrumentation or the finite distance between accelerometer and microphone introduces a time delay Δt between pressure and velocity signals, this is related to a phase shift Φ by $\Delta t = \Phi/2\pi f$, where f is the frequency, in Hz. The intensity is usually computed in the frequency domain by feeding the velocity and pressure signals into an *FFT* analyzer, since the spectral distribution of sound power is usually required. The acoustic intensity may be shown to be [25, 26]:

$$I_n = \int_0^\infty [C_{up}(f)\cos\Phi + Q_{up}(f)\sin\Phi]\,df, \tag{9}$$

where C_{up} is the co-spectrum (real part) and Q_{up} is the quad-spectrum (imaginary part) of the one-sided cross-spectral density between velocity and pressure G_{up};

$$G_{up}(f) = C_{up}(f) - iQ_{up}(f). \tag{10}$$

McGary and Crocker continued development of the surface intensity technique [28-31]. They then applied it successfully to the determination of the sound intensity radiated from the different surfaces of a Cummins NTS 350 diesel engine [28, 29, 31]. This work is described in section 6.4 of this paper. Use of the velocity signal in this analysis, however, is rather inconvenient, since an along integrator is needed to integrate the signal produced by the accelerometer. It is simpler to eliminate use of the velocity signal through mathematical techniques and use instead the acceleration signal. The equation for intensity, I, then becomes

$$I = (1/2\pi) \int_0^\infty (1/f)(Q_{pa}\cos\Phi + C_{pa}\sin\Phi)\,df, \tag{11}$$

where Q_{pa} is the imaginary part of the one-sided cross-spectral density between pressure and acceleration, C_{pa} the real part of the one-sided cross-spectral density between pressure and acceleration and Φ the instrumentation phase shift. This was the approach used by McGary and Crocker in the measurements described in section 5.4 of this paper.

5.3 Noise source identification using the lead-wrapping technique

The selective-wrapping approach used in conjuction with the selective-operation approach have been the basic methods used to noise-source identify engines and other machines until very recently. Since the normal procedure now is to use a lead barrier enclosure with acoustic absorbing material between the lead and the engine, the approach is often also called lead-wrapping. It has been assumed by many people until recently that this approach will give the most reliable method of identifying noise source on the surface of a machine and it has been used as a baseline against which other approaches are compared.

In the work by Crocker *et al.* [28, 29, 36, 37, 40, 51] described in the present paper, measurements on a diesel engine using the lead-wrapping approach were used as a baseline against which to compare measurements made with the intensity techniques. The floor of the Herrick Laboratories semi-anechoic room was covered with fiberglass wedges and a hoop was rotated around a Cummins NTC 350 HP diesel engine. First the intensity I was obtained at thirty measurement points on the hoop traverse by assuming the far field approximation

$$I = p_{\text{rms}}^2/\varrho c, \tag{12}$$

where p_{rms}^2 is the mean square sound pressure measured, ϱ is the air density and c is the speed of sound. Then, the sound power W was obtained by sum-

mation over the spherical area S covered by the hoop traverse around the engine using equation (8), where dS is the incremental area associated with each microphone position.

It has been shown during the present research that the lead-wrapping approach has several serious drawbacks. First, the lead-wrapping method is time-consuming, tedious and expensive. Second, a special facility: an anechoic engine-test cell is really required to obtain accurate, reliable results. Third, the method fails at low frequency (below about 200 to 300 Hz) because the lead becomes "transparent" to engine noise. This is obvious if mass law transmission loss theory is studied. In addition, since the lead is situated close to the engine wall it may act as a tight-fitting enclosure and actually amplify the engine noise at low frequency. See the measurements of the sound power of the bare engine and fully-wrapped engine given in Fig. 8. The net effect is that at low

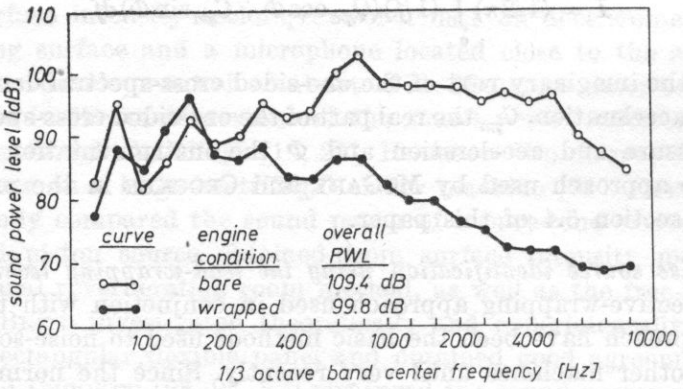

Fig. 8. Comparison of the sound power level of the bare engine and the fully-wrapped engine measured at 1500 rpm and 542 Nm load

frequency it is difficult to separate the noise of one engine part from the total engine noise. See, for example, the measured sound power of the oil pan (sump) in Fig. 9. The oil pan is a strong source on this engine. A fourth and related drawback is that the lead-wrapping method works well only for the stronger noise source on the engine surface. When a surface, which is only a moderate or weak source of sound, is exposed it is difficult or impossible to determine its contribution accurately except in the very high frequency range (several thousand Hz). See, for example, Fig. 10 which shows the sound power of the fuel and oil pumps (a weak source on this engine). The measurements in Figs. 8-10 were made by rotating microphones on a hoop around a lead-wrapped Commins NTC 350 diesel engine in the semi-anechoic room at Herrick Laboratories (see Fig. 11). The engine was mounted at a height of about 1.5 m above the foor so that the hoop could be easily rotated around it [28, 29, 36, 37, 40, 51].

5.4 Comparison between surface intensity and lead-wrapping measurements
The sound power radiated from 5 different surfaces of the Cummins engine was measured using the surface intensity technique and compared with the sound power radiated from the same surfaces determined from the lead-wrapping approach [28, 29].

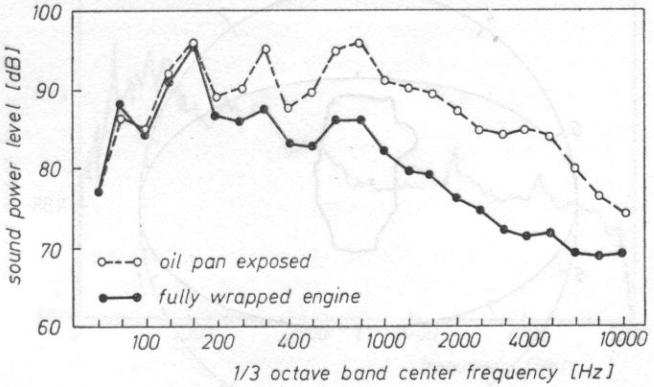

Fig. 9. Comparison of the sound power level of the oil pan and the fully-wrapped engine measured at 1500 rpm and 542 Nm load

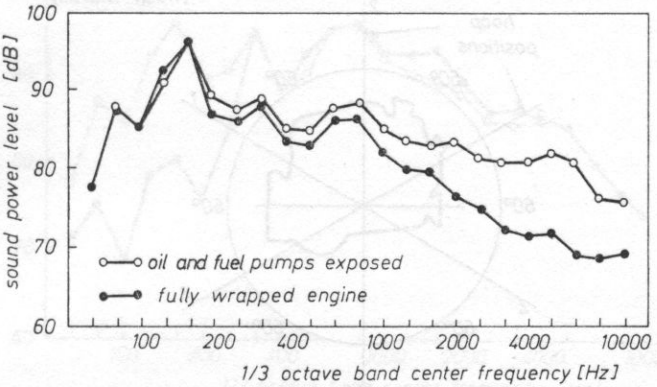

Fig. 10. Comparison of the sound power level of the fuel and oil pumps with that of the fully-wrapped engine measured at 1500 rpm and 542 Nm load

The five parts chosen for surface intensity measurements were: 1) the oil pan, 2) the after-cooler, 3) the left block wall, 4) the right block wall, and, 5) the oil filter and cooler. The exhaust manifold and cylinder head were not investigated because of the intense heat radiated by these parts. High surface temperatures can make acceleration readings difficult or inaccurate and are somewhat dangerous for investigators moving the accelerometer from location to location. The front of the engine was not examined either, because pulleys there made

it very difficult to mount an accelerometer and locate the microphone. Figs. 12 and 13 show the sound power obtained by summing over 24 locations on the oil pan using equation (8). Fig. 12 shows narrow band results, while Fig. 13 shows the narrow band sound power results presented in Fig. 12 summed into

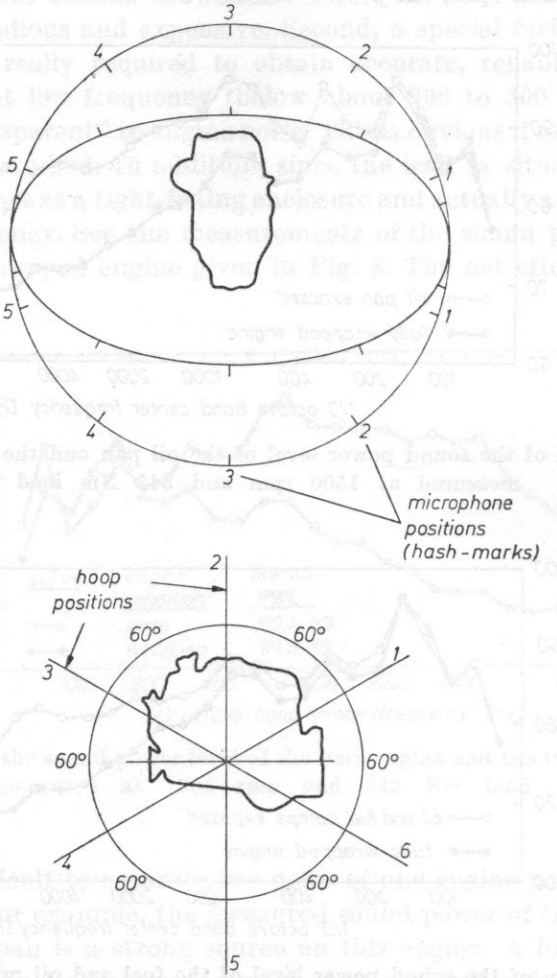

Fig. 11. Microphone positions on hoop which was rotated around engine for sound power measurements

one-third octave bands. The curve with symbols O was obtained from the lead-wrapping method, while the curve with symbols S was obtained from the surface intensity technique. The results for the other four surfaces examined on the engine are given in references [28, 29].

It is seen in Fig. 13 that the agreement between the two methods is good except at very low frequency (below 315 Hz). At low frequency the lead becomes

"transparent" to sound as already discussed and the surface intensity method is less accurate because of calibration difficulties [30]. The trend for the lead-wrapping results to be higher than the surface intensity results in the lower frequency region was observed for all the five parts examined and is as expected.

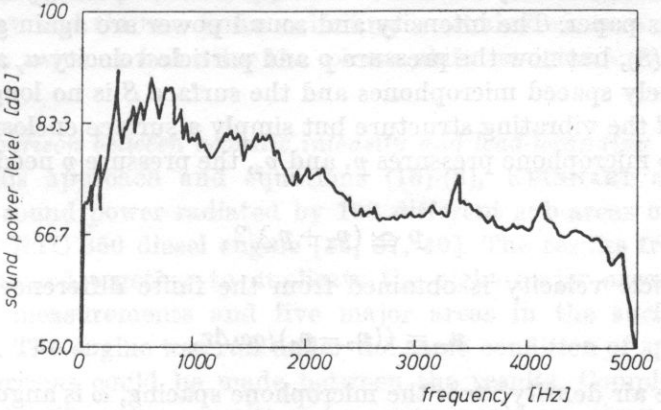

Fig. 12. Narrow band sound power level determined from surface intensity method summed over 24 sub-areas of the surface of the oil pan measured at 1500 rpm and 542 Nm load

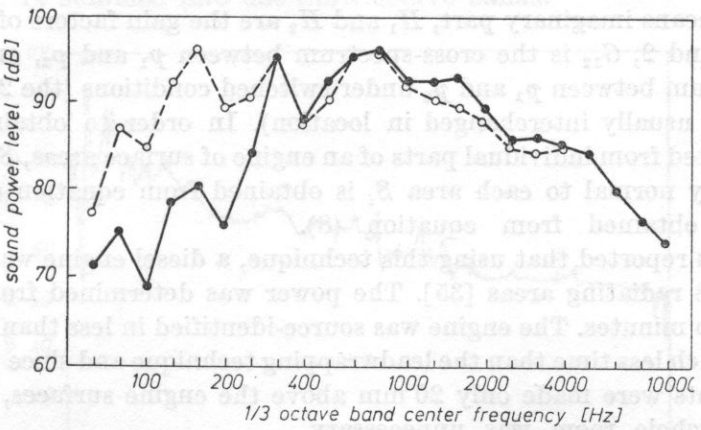

Fig. 13. Comparison of sound power level determined for the oil pan from the spherical traverse lead-wrapping technique ○——○ and the sound power level from the surface intensity method ●——●

5.5 Noise source identification using the acoustic intensity technique

The measurement of acoustic intensity has been possible since the last century using Rayleigh's disc. However, Rayleigh's disc is impractical in noise work. In the last fifty years several workers have investigated the measurement of acoustic intensity using various two-microphone devices. OLSEN in 1932 took out a patent for its measurement. At last it appears that the *FFT* analyzer

has now made practical intensity measurements possible. Recent developments suggest that acoustic intensity measurements are quicker and at least as accurate as the selective wrapping approach in measuring engine noise sources.

FAHY [32, 33] and CHUNG [34, 35] have given the theory for the measurement of acoustic intensity similar to that for surface intensity in the previous section of this paper. The intensity and sound power are again given by equations (7) and (8), but now the pressure p and particle velocity u_r are determined with two closely spaced microphones and the surface S is no longer necessarily the surface of the vibrating structure but simply a surface enclosing the source. From the two microphone pressures p_1 and p_2, the pressure p needed in equation (7) is

$$p \cong (p_1+p_2)/2, \tag{13}$$

and the particle velocity is obtained from the finite difference assumption

$$u_r = i(p_2-p_1)/\varrho\omega\Delta r, \tag{14}$$

where ϱ is the air density, Δr is the microphone spacing, ω is angular frequency. By substituting equations (13) and (14) into (7), CHUNG [34, 35] showed that

$$I_r = \mathrm{Im}\{[G_{12}G_{12}^S]^{1/2}\}/\varrho\omega\Delta r\,|H_1|\,|H_2|, \tag{15}$$

where Im means imaginary part, H_1 and H_2 are the gain factors of microphone systems 1 and 2, G_{12} is the cross-spectrum between p_1 and p_2, and G_{12}^S is the cross-spectrum between p_1 and p_2 under switched conditions (the 2 microphone systems are usually interchanged in location). In order to obtain the sound power radiated from individual parts of an engine of surface areas, $S_1, S_2, \ldots, S_N$, the intensity normal to each area S_i is obtained from equation (15) and the power W obtained from equation (8).

CHUNG reported that using this technique, a diesel engine was subdivided into $N = 98$ radiating areas [35]. The power was determined from each area in about two minutes. The engine was source-identified in less than a day which involved much less time than the leadwrapping technique and since the intensity measurements were made only 20 mm above the engine surfaces, an anechoic or semi-anechoic room was unnecessary.

REINHART and CROCKER [36, 37] did not use the intensity formulation given in equation (15) but rather that suggested by KRISHAPPA [38] and ROLAND [39]. In this formulation the acoustic intensity is

$$I_r = \mathrm{Im}\{G_{12}\}/\varrho\omega\Delta r. \tag{16}$$

Corrections for phase shift between the two microphone channels are made using equation (17). The true cross spectrum G_{12} between the microphone signals is related to the measured value G'_{12} by

$$G'_{12} = G_{12}T_{12}/|H_1|^2, \tag{17}$$

where T_{12} is the transfer function between microphone channel systems 1 and 2 and (H_2) is the gain of microphone system 2. In this phase shift determination, the two microphones were mounted at the same longitudinal position at the end of a small tube which was excited by a white noise source from a small loudspeaker. In principle, this approach has some advantage over that suggested by FAHY and CHUNG. Since switching is eliminated, measurements can be made about twice as fast after the phase shift is determined and stored on the *FFT*.

5.6 Comparison between acoustic intensity and lead-wrapping measurements

Using this approach and equations (16)-(8), REINHART and CROCKER measured the sound power radiated by 103 different sub-areas on the surface of a Cummins NTC 350 diesel engine [36, 37, 40]. The results from groups of areas were summed together to duplicate the eight major areas used in the lead-wrapping measurements and five major areas in the surface intensity measurements. The engine was run under the same condition of speed and load so that comparisons could be made between the results. Complete details of the acoustic intensity engine results and measurements are given in [40]. Figs. 14 and 15 show the sound power obtained by summing over 25 locations on the oil pan. Fig. 14 shows narrow band results while Fig. 15 shows the results given in Fig. 14 summed into one-third octave bands.

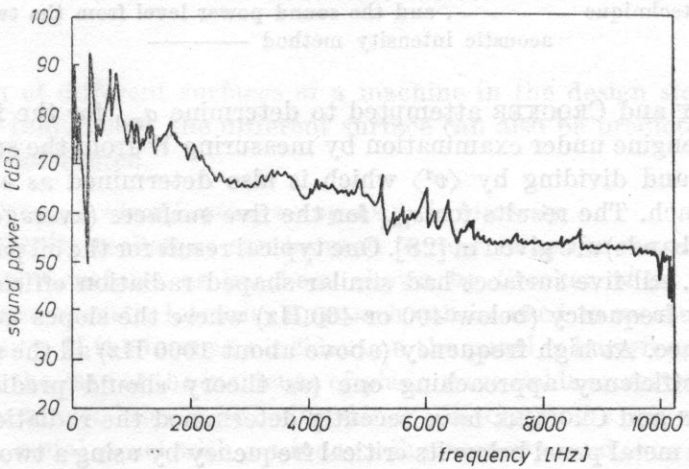

Fig. 14. Oil pan narrow-band sound power level spectrum determined from two-microphone acoustic intensity method. (Peaks occur at 300 Hz, 650 Hz and 790 Hz. All intensity measurements were made at an engine speed of 1500 rpm and a load of 542 Nm)

It is interesting to note some peaks in the narrow band spectrum in Fig. 14 which are presumably caused by a forcing frequency being close to a structural resonance frequency. Also of interest is the good agreement between the lead-wrapping and the acoustic intensity results in Fig. 15 for frequencies at and

above 315 Hz. This result is similar to that for the oil pan when the lead-wrapping and the surface intensity results were compared in the previous section of this paper. The results for the other major engine surfaces are given in [37] and [40].

5.7 Radiation efficiency of different machine surfaces

The sound power W_{rad} radiated by a vibrating surface of area S is given by equation (1) in section 3.2 of this paper.

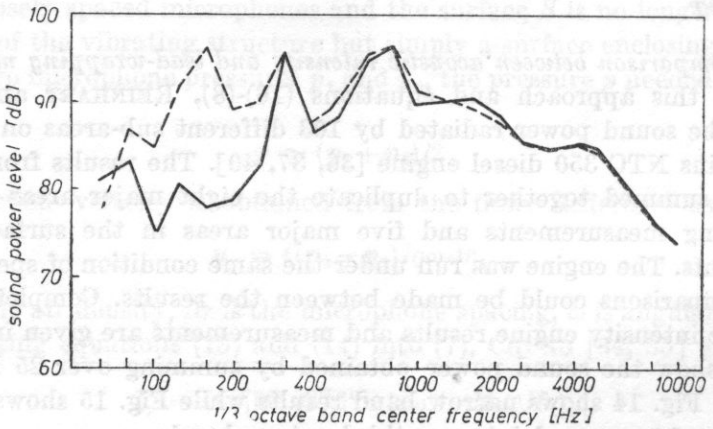

Fig. 15. Comparison of sound power level determined for the oil pan from the spherical lead-wrapping technique — — — —, and the sound power level from the two-microphone acoustic intensity method ————

McGary and Crocker attempted to determine σ_{rad} for the five surfaces of the diesel engine under examination by measuring W from the surface intensity method and dividing by $\langle v^2 \rangle$ which is also determined as a by-product of this approach. The results for σ_{rad} for the five surfaces (averaged over one-third octave bands) are given in [28]. One typical result for the oil pan is presented in Fig. 16. All five surfaces had similar shaped radiation efficiency curves, except at low frequency (below 400 or 400 Hz) where the slopes were different for each surface. At high frequency (above about 1000 Hz) all the surfaces had a radiation efficiency approaching one (as theory should predict).

Forssen and Crocker have recently determined the radiation efficiency of a vibrating metal panel below its critical frequency by using a two microphone method [41, 42]. The sound power W_{rad} was obtained with the two microphone acoustic intensity technique using equation (16) which was summed over the panel area with equation (8). The panel surface velocity was obtained by placing the two-microphone probe very close to the panel surface and moving it over the panel surface to obtain $\langle v^2 \rangle$. Finally, the radiation efficiency σ_{rad} was calculed from equation (1). See [41, 42].

Such radiation efficiency curves, if they can be accurately predicted or measured, can be very useful in machine design in a number of ways. They

enable an experimentalist to determine the sound power radiated by each machine surface, simply by measuring the space-averaged mean-square velocity (as a function of frequency) on that surface. This can easily be accomplished using an accelerometer rather than making a complicated or sophisticated intensity or sound power measurement. Also, in principle, if theory can be used to predict

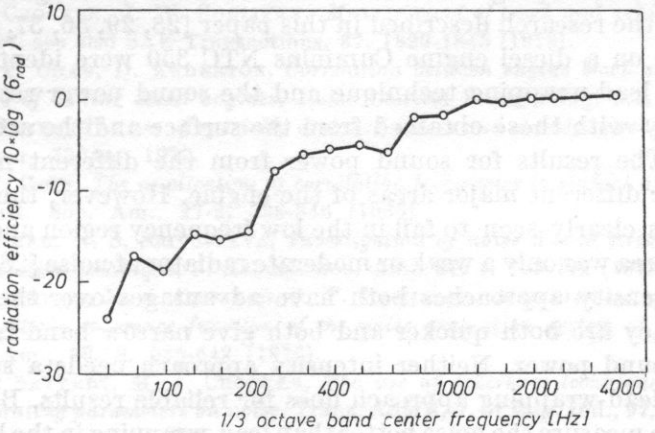

Fig. 16. Radiation efficiency of the oil pan determined at an engine speed of 1500 rpm and a load of 542 Nm

the vibration of different surfaces of a machine in the design stage, then the sound power radiated by the different surface can also be predicted before the machine is constructed.

5.8 Noise path identification using acoustic intensity

The intensity technique can be used to determine the sound transmitted through panel structures as has been shown by Crocker *et al.* [43-47]. The two-microphone acoustic intensity approach can be used to measure the transmitted intensity. If the intensity incident on the panel is known or can be measured (e.g. in the case of the incidence of plane wave fields or reverberant fields) then the transmission loss can be deduced immediately. In the case of a composite panel (e.g. a metal panel with a window) the intensity (and thus sound power) transmitted through the metal wall and the window can be measured separately. Thus the sound power transmitted by the wall path and the window path can be distinguished. This has important applications in attempting to determine noise paths in buildings and aircraft structures. Villot and Roland have used this intensity approach successfully to attempt to distinguish between direct and flanking paths in buildings [48]. McGary and Hayes [49] have successfully separated airborne and structure-borne noise paths in aircraft-like structures using the intensity approach.

6. Conclusions

The earlier methods of identifying noise source and paths reviewed in this paper are still useful. However the new intensity techniques promise to become very important in identifying noise sources and paths. The surface intensity (accelerometer-microphone and acoustic intensity (two-microphone) techniques of identifying noise sources have been investigated and further developed in the research described in this paper [28, 29, 36, 37, 40]. The major noise sources on a diesel engine Cummins NTC 350 were identified using the conventional lead-wrapping technique and the sound power results were compared directly with those obtained from the surface and the acoustic intensity techniques. The results for sound power from the different methods agreed quite well for different major areas of the engine. However, the lead-wrapping approach was clearly seen to fail in the low frequency region and also when the noise source area was only a weak or moderate radiator of noise [28, 29, 36, 37, 40].

The intensity approaches both have advantages over the lead-wrapping approach. They are both quicker and both give narrow band frequency information on sound power. Neither intensity approach needs a special anechoic room as the lead-wrapping approach does for reliable results. Both approaches can be used to measure the noise better than lead-wrapping in the lower frequency region and when the source areas are weaker noise radiators. Of the two intensity approaches, the acoustic intensity approach is clearly quicker if the two-microphone array can be hand-held. For safety reasons this is not always possible. However, the surface intensity approach has the advantage over the acoustic intensity approach, in that radiated acoustic power, surface velocity and radiation efficiency information are obtained simultaneously. In addition, the velocity being determined from a transducer measurement in the surface intensity approach is not subject to the same low and high frequency errors as in the acoustic intensity approach (see equation (14)). At low frequency, difficulty with equation (14) is encountered since p_1 and p_2 are almost identical. At high frequency again equation (14) predicts erroneous results when $(\omega/c)\Delta r \rightarrow 1$. The two-microphone method can also be used to estimate the velocity of a vibrating surface and to determine the sound transsmision paths through wall structures. The intensity techniques hold the promise of very wide application in many machinery noise problems.

References

[1] M. J. Crocker, *Sources of noise in diesel engines and the prediction of noise from experimental measurements and theoretical models*, INTER-NOISE 75 Proceedings, 1975, pp. 259-266.

[2] M. J. Crocker, *Reduction of diesel engine noise in trucks*, 1976, Noise Control Reference Proceedings, Warsaw, pp. 1-11.

[3] M. J. Crocker, *Identification of noise from machinery, review and novel methods*, INTER-NOISE 77, Proceedings, 1977, pp. A201-211.

[4] R. L. Staadt, *Truck noise control*, in: *Reduction of machinery noise*, Proceedings, Purdue University, 1975, pp. 158, 190.

[5] M. J. Crocker, J. F. Hamilton, *Modeling of diesel engine noise using coherence*, SAE Paper 790362, see also SAE Transactions, **88**, 1263-1273 (1980).

[6] P. François, *Isolation et revetements*, Les Cartes de Niveaux Sonores, pp. 5-17 (January-February 1966).

[7] M. J. Crocker, J. W. Sullivan, *Measurement of truck and vehicle noise*, 1978, SAE Paper 780387, see also SAE Transactions, **87**, 1829-1845 (1979).

[8] C. M. P. Chan, D. Anderton, *Correlation between engine block surface vibration and radiated noise of in-line diesel engines*, Noise Control Engineering, 2.1, 16-24 (1974).

[9] G. E. Thien, *The use of specially designed covers and shields to reduce diesel engine noise*, SAE Paper 73044, 1973.

[10] K. W. Goff, *The application of correlation techniques to surface acoustical measurements*, J. Acoust. Soc. Am., 27-2, 336-346 (1955).

[11] S. Kumar, N. S. Srivastava, *Investigation of noise due to structural vibrations using a cross-correlation technique*, J. Acoust. Soc. Am., **57**, 4, 769-772 (1975).

[12] J. Y. Chung, M. J. Crocker, J. F. Hamilton, *Measurement of frequency responses and the multiple coherence function of the noise generation system of a diesel engine*, J. Acoust. Soc. Am., **58**, 3, 635-642 (1976).

[13] A. F. Seybert, M. J. Crocker, *The use of coherence techniques to predict the effect of engine operating parameters on noise*, Trans. ASME, J. of Eng. Ind., **97**, B, 4, 1227-1233 (1976).

[14] A. F. Seybert, M. J. Crocker, *Recent applications of coherence function techniques in diagnosis and prediction of noise*, INTER-NOISE 76 Proceedings, 1976, pp. 7-12.

[15] A. F. Seybert, M. J. Crocker, *The effect of input cross-spectra on the estimation of frequency response functions in certain multiple-input systems*, Archives of Acoustics, 3, 3, 3-23 (1978).

[16] P. A. Hayes, A. F. Seybert, J. F. Hamilton, *A coherence model for piston-impact generated noise*, SAE Paper 790274.

[17] M. E. Wang, *The application of coherence function techniques for noise source identification*, Ph. D. Thesis, Purdue University, 1978.

[18] M. E. Wang, M. J. Crocker, *Recent applications of coherence techniques for noise source identification*, INTER-NOISE 78 Proceedings, 1978, pp. 375-382.

[19] J. A. Macadam, *The measurement of sound power radiated by individual room surfaces in lightweight buildings*, Building Research Establishment, Current Paper 33174, 1974.

[20] J. A. Macadam, *The measurement of sound radiation from room surfaces in lightweight buildings*, Applied Acoustics, **9**, 2, 103-118 (1976).

[21] T. H. Hodgson, *Investigation of the surface intensity method for determining the noise sound power of a large machine in situ*, J. Acoust. Soc. Am., **61**, 2, 487-493 (1977).

[22] S. Czarnecki *et al.*, *Correlation method of measurements of sound power in the near field conditions*, Archives of Acoustics, **1**, 3, 201-213 (1976).

[23] J. D. Brito, *Sound intensity patterns for vibrating surfaces*, Ph. D. Thesis, MIT, 1976.

[24] J. D. Brito, *Machinery noise source analysis using surface intensity measurements*, NOISE-CON 79 Proceedings, 1979, pp. 137-142.

[25] N. Kaemmer, *Determination of sound power from intensity measurements on a cylinder*, MSME Thesis, Purdue University, 1978.

[26] N. Kaemmer, M. J. Crocker, *Surface intensity measurements on a vibrating cylinder*, NOISE-CON 79 Proceedings, 1979, pp. 153-160.

[27] N. KAEMMER, M. J. CROCKER, *Sound power determination from surface intensity measurements on a vibrating cylinder*, J. Acoust. Soc. Amer., 1983.

[28] M. MCGARY, M. J. CROCKER, *Noise source identification of diesel engines using surface intensity measurements*, EPA Contract 68-01-4907, Report No. 5, HL 80-2, January 1980.

[29] M. MCGARY, M. J. CROCKER, *Surface intensity measurents on a diesel engine*, Noise Control Engineering, **16**, 1, 26-36 (1981).

[30] M. MCGARY, M. J. CROCKER, *Correction of instrumentation phase shift errors in the theory and practice of surface acoustical intensity measurements*, J. Sound Vib., **82**, 2, 275-288.

[31] M. MCGARY, M. J. CROCKER, *Surface acoustical measurements on a diesel engine*, NASA Technical Memorandum 81807, April 1980.

[32] F. J. FAHY, *Measurement of the acoustic intensity using the cross-spectral density of two microphone signals*, J. Acoust. Soc. Am., **62**, 4, 1057-1059 (L) (1977).

[33] F. J. FAHY, *A Technique for measuring sound intensity with a sound level meter*, Noise Control Engineering, **9**, 3, 155-161 (1977).

[34] J. Y. CHUNG, *Cross-spectral method of measuring acoustic intensity without error caused by instrument phase mismatch*, J. Acoust. Soc. Amer., **64**, 6, 1613-1616 (1978).

[35] J. Y. CHUNG *et al.*, *Application of acoustic intensity measurement to engine noise evaluation*, SAE Paper 790502, 1979.

[36] T. E. REINHART, M. J. CROCKER, *A comparison of noise source identification techniques on a diesel engine*, INTER-NOISE 80 Proceedings 1980, 1129-1132.

[37] T. E. REINHART, M. J. CROCKER, *Source identification on a diesel engine using acoustic intensity measurements*, Noise Control Engineering, **18**, 3, pp. 84-92 (1982).

[38] G. KRISHNAPPA, *Cross-spectral method of measuring acoustical intensity – correcting phase mismatch error by calibrating two microphone systems*, J. Acoust. Soc. Am., Suppl. 1, **66**, S39, J. Acoust. Soc. Am., **69**, 1, 307-210 (1981).

[39] J. ROLAND, M. J. CROCKER, M. SANDBAKKEN, *Problems with in-duct measurement of fan sound power using* ASHRAE *research project RP-***264**, Final Report, March 1981.

[40] T. E. REINHART, M. J. CROCKER, *Noise source identification of diesel engines using acoustic intensity measurements*, EPA Contract 68-01-4907, Report No. 7, HL 80-39, September 1980.

[41] B. FORSSEN, M. J. CROCKER, *Estimation of surface velocity by use of the two microphone technique*, Proceedings of INTER-NOISE 82, 1982, II, pp. 689-690.

[42] B. FORSSEN, M. J. CROCKER, *Estimation of acoustic velocity, surface velocity and radiation efficiency by use of the two-microphone technique*, J. Acoust. Soc. Amer., 1983.

[43] M. J. CROCKER, B. FORSSEN, P. K. RAJU, A. MIELNICKA, *Measurement of transmission loss of panels by an acoustic intensity technique*, INTER-NOISE 80 Proceedings, 1980, pp. 741-746.

[44] M. J. CROCKER, P. K. RAJU, B. FORSSEN, *Measurement of transmission loss of panels by the direct determination of transmitted acoustic intensity*, Noise Control Engineering, **17**, 1, 6-11 (1981).

[45] Y. S. WANG, M. J. CROCKER, P. K. RAJU, *Theoretical and experimental evaluation of transmission loss of cylinders*, Paper No. AIAA 81-1971, AIAA Seventh Aeroacoustics Conference, Palo Alto, California; AIAA Journal, 1983.

[46] Y. S. WANG, M. J. CROCKER, *Direct measurement of trnasmission of aircraft structures using acoustic intensity approach*, Proceeding of INTER-NOISE 82 1982, II, 687-690.

[47] Y. S. WANG, M. J. CROCKER, *Direct measurement of transmission loss of aircraft structures using acoustic intensity approach*, Noise Control Engineering, **19**, 3, pp. 80-85 (1982).

[48] M. VILLOT, J. ROLAND, *Measurement of sound powers radiated by individual room surfaces using the acoustic intensity method*, Proceedings of the International Congress

on Recent Developments in Acoustic Intensity Measurement, Senlis, France, 1981, pp. 153-159.

[49] M. C. McGary, W. H. Hayes, *A new measurement technique for separating airborne and structure-borne aircraft interior noise*, Noise Control Engineering, **20**, 1, 21-30 (1983).

[50] S. P. Ying, E. E. Dennison, *Application of coherence technique for noise in power plants*, Noise Control Engineering **15**, 2, 81-87 (1980).

[51] M. J. Crocker, *Comparison between surface intensity, acoustic intensity and selective wrapping noise measurements on a diesel engine*, in R. Hickling and M. M. Kammal (*Eds*), *Engine noise, excitation, vibration, and radiation*, Plenum Press, New York 1982, pp. 279-311.

Received on 9 March, 1983

ARCHIVES OF ACOUSTICS
8, 4, 317-330 (1983)

SELF-EXCITED FLOW OSCILLATION IN AN ABRUPTLY EXPANDING CIRCULAR DUCT AS THE NOISE SOURCE

ANDRZEJ P. SZUMOWSKI, JANUSZ PIECHNA

Institute of Aircraft Technology and Applied Mechanics, Warsaw Technical University (00-665 Warsaw, ul. Nowowiejska 24)

The behaviour of oscillations in subsonic flow in a duct with a sudden enlargement of cross-section has been investigated experimentally. The mechanism of one type of oscillation has been found and explained. In this type of oscillation the resonant oscillation of a gas column in the part of a duct with constant cross-section is sustained by flow in the extended part of the duct. The flow is accompanied by periodically occurring and downstream moving annular vortices which close the feedback loop. The shadow graph visualization has confirmed the existence of this coherent vortex structure in the flow.

1. Introduction

In internal flows a rapid expansion of the cross-section of the duct causes flow separation and the occurence of stagnation regions. Such a configuration is not stable and very often induces self-excited flow oscillations which generate loud noise. The mechanism of such oscillations is frequently defined as the acoustic-flow feedback.

The group of flows in which oscillations can occur includes flows past cavities [1-3], orifices [4], expansion chambers [5] and ducts with rapid change in cross-section [6-9]. The object of the investigation presented here is self-excited oscillation occurring in subsonic flow in an outlet with a sudden cross-section increase at the end. Some experimental studies [6, 7] have been devoted to this phenomenon. The authors have considered this problem only from the point of view of technical application. Oscillation of such a type increases the jet mixing rate, so that the operation of various kinds of ejectors can be improved. No investigators have paid much attention to the mechnism of this oscillation. It has only been suggested that the jet periodically separates and

reattaches to the wall of the expanded part of the duct. Previous investigators [8, 9] of oscillation in supersonic flow in similar configurations have shown that depending on the pressure difference at both ends of the duct several types of oscillation can occur. One can expect that many types of oscillation can also exist in subsonic flow.

Thus, the investigations reported on in this paper focused on the study of the mechanism of oscillation in subsonic flow in a duct with a relatively short collar and relatively low gas velocity.

2. Investigation facility

Fig. 1a shows a schematic diagram of the investigation facility. Air with controlled supply pressure (p_0) flows to a chamber lined with some absorbing material, in order to reduce partially the initial flow turbulence. From the

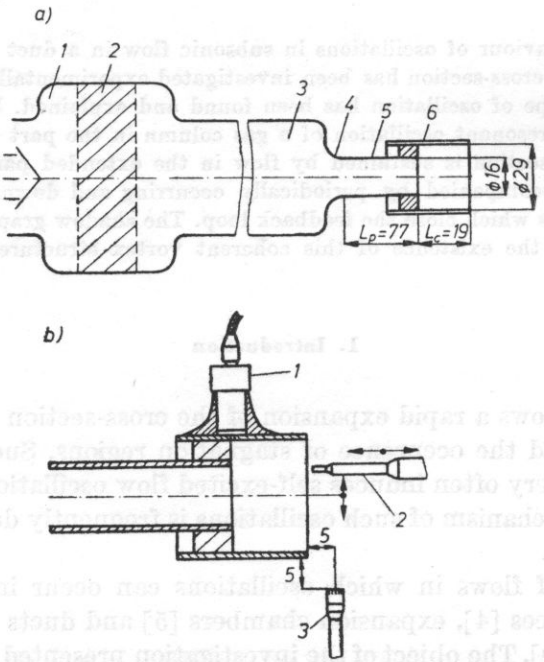

Fig. 1. A schematic diagram of the experimental facility

a) *1* – chamber, *2* – damping element, *3* – supply duct, *4* – nozzle, *5* – duct, *6* – collar; b) *1* – pressure transducer, *2* – thermoanemometer probe, *3* – microphone

chamber the air flows out through a duct with a relatively large cross-section to a convergent nozzle at the end. The nozzle is fastened by a duct with a movable collar, forming a channel with a sudden increase of cross-section.

The arrangement of the measuring equipment is shown in Fig. 1b.

Acoustic measurements were carried out with *B* and *K* equipment, using for spectral analysis a 2010 narrow-band analyser and a 2307 recorder. A 4133 1/8″ microphone with a 2619 preamplifier was placed in the near field (see Fig. 1b). The pressure pulsation inside the collar was measured using a Kistler (7031) piezoelectric transducer with a 5007 charge amplifier. Flow velocity measurements were carried out with a 55 *MOI* bridge and a 55 *D*10 linearizer. The cross correlation between the pressure and the flow velocity signal was performed by a 55 *D*70 *DISA* correlator with normalisation of input signals. The correlation functions were recorded on a 411 Watanabe recorder.

3. Results of measurements

The noise from such a type of flow oscillation was very distinct. Fig. 2 shows the spectra of sound emitted by the air flow in three different configurations (free jet, short collar and long collar). All measurements were carried

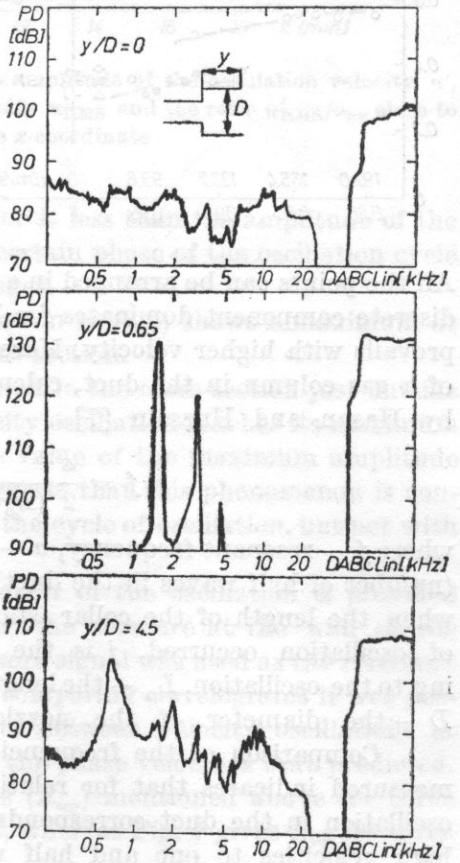

Fig. 2. Sound spectra

out for the same ratio of the ambient to the stagnation pressure (0.95), corresponding to flow velocity of 93 m/s. Strong flow pulsation occurred only for the duct with a short collar. The overall sound level was in this case about 30 dB higher than that for the other configurations. The noise spectrum showed a distinct discrete component and its harmonics.

Fig. 3 shows the dimensionless frequency of the sound spectrum versus the pressure ratio of flow velocity. The dark points mark the dominant components.

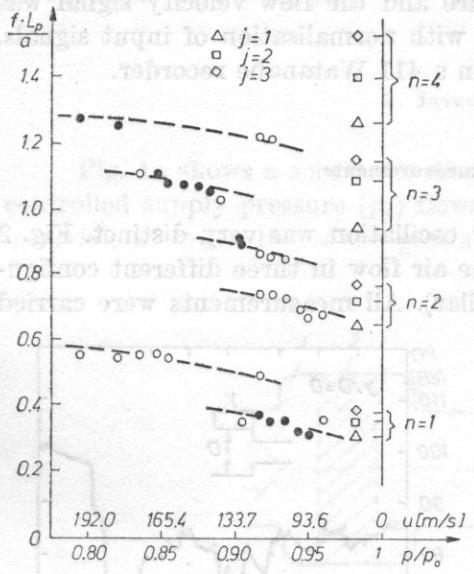

Fig. 3. Dominant frequencies in the sound spectrum

All the points can be arranged in a number of bands. The first harmonic of the discrete component dominates for lower flow velocity, whereas the second one prevails with higher velocity. Moreover, Fig. 3 shows the resonant frequencies of a gas column in the duct, calculated from the experimental formula given by Hasan and Hussain [7]

$$f = \frac{a}{2} \frac{n}{(L_p + 1.65 L_c/j + 0.7D)},$$

where f — resonant frequency, a — the speed of sound, n — mode of operation (number of half waves in the duct), j — stage of operation defined as follows: when the length of the collar (starting from zero) was increased some range of oscillation occurred, j is the number of successive ranges corresponding to the oscillation, L_p — the length of the nozzle, L_c — the length of the collar, D — the diameter of the nozzle.

Comparison of the frequencies calculated from this formula and those measured indicates that for relatively low velocities the mode of resonance oscillation in the duct corresponds to half the wavelength and for relatively high velocities to one and half wavelengths.

The properties of the sound spectrum considered here are strictly connected with flow oscillation in ducts.

Fig. 4. gives the results of flow velocity measurements along the wall of the collar. The mean flow velocity at the wall is negative (the flow is from

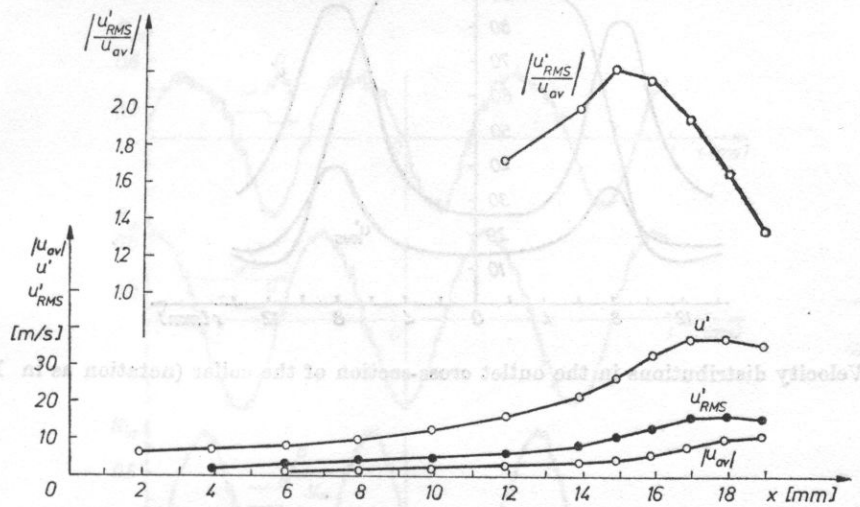

Fig. 4. Distributions of the mean velocity u_{av}, the amplitude of the oscillation velocity u', the rms value of the amplitude of oscillation velocity u'_{RMS} and the ratio u'_{RMS}/u_{av} close to the collar versus the x-coordinate

the surroundings into the collar) and its value is less than tha amplitude of the velocity oscillation. This singnifies that in a certain phase of the oscillation cycle the direction of the flow in this region changes.

The relative amplitude velocity oscillation (u'/u_{av}) shows a maximum at a position 4 mm from the collar outlet cross-section.

Fig. 5 presents velocity profiles measured in the cross-section just outside the collar outlet. The amplitude of the velocity oscillation reaches its maximum value at the boundary of the jet. The large value of the maximum amplitude is very close to the mean velocity. This suggests that this phenomenon is connected with variation of the jet diameter in the cycle of oscillation, but not with turbulence.

Essential information about the character of the oscillation is provided by the function of cross correlation between the pressure at the wall of the collar (Fig. 1b) and flow velocities. The pressure signal was used as the reference signal in the correlation measurements. By comparing correlograms it was possible to determine the relative phase shifts between velocity oscillations at different points of the flow field. In this way the phase velocities were predicted.

Fig. 6 shows the correlation functions (R_{up}) mentioned above for three points in the outlet cross-section of the duct, whereas Fig. 7 gives R_{up} for three

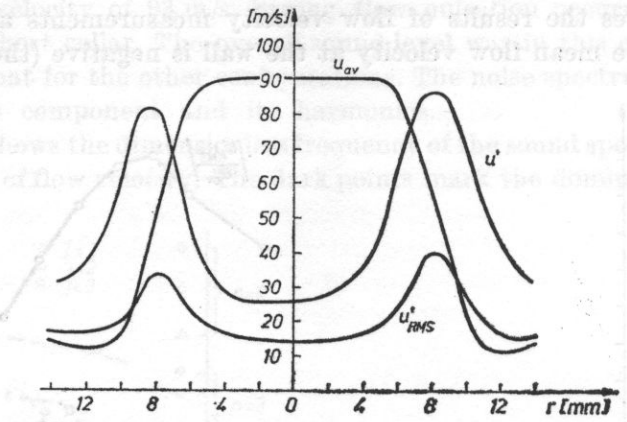

Fig. 5. Velocity distributions in the outlet cross-section of the collar (notation as in Fig. 4)

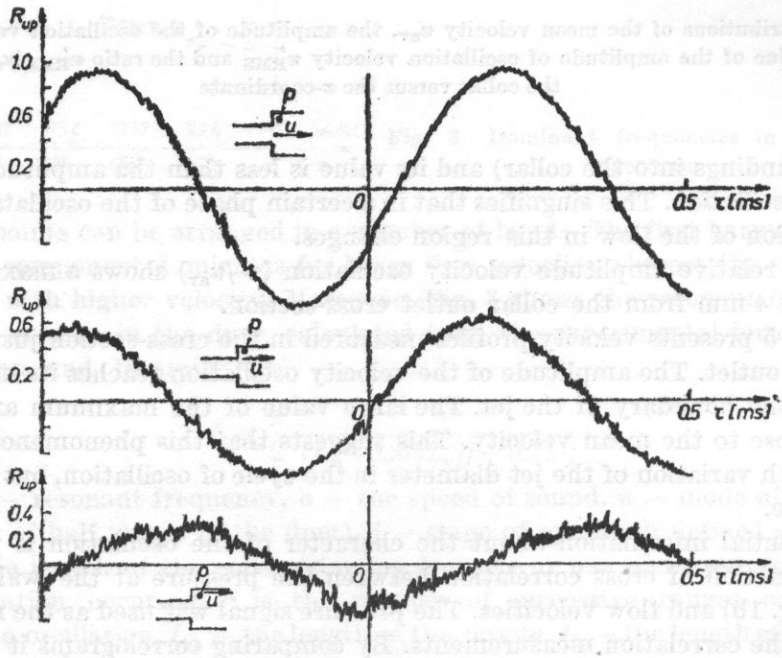

Fig. 6. Correlograms of the pressure trace in the collar and velocity traces in the cross-section close to the outlet of the duct

points in the outlet cross-section of the collar. At the axes of the abscissae of all these figures there are time delays (τ) between correlated signals. The positive value of τ denotes the delay of the velocity signal with respect to the pressure signal.

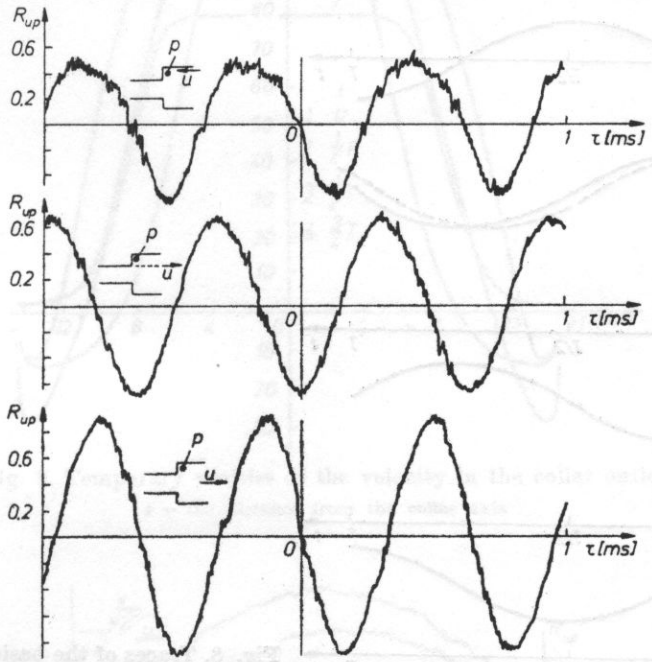

Fig. 7. Behaviour of the pressure correlation factor and velocity in the outlet cross-section of the collar

The following conclusions can be drawn from these correlation functions.

Correlograms have a distinctly harmonic character, which proves the existence of strong discrete components in the measured traces of the pressure and velocities. The values of the correlation functions are the greatest for velocities at the points along the axis of the duct. It indicates the least contribution of random components to this phenomenon. On the basis of the correlation functions the phase shifts between the basic flow parameters were found.

Fig. 8. shows the change in the main flow properties in one cycle of oscillation. All these lines were deduced from an analysis of the correlograms and velocity measurements. The approximate values of the phase shift between velocity signals at some points of the flow field and the reference pressure signal, corresponding to Fig. 8, are given in Table I. On the basis of the results of measurements given above, the temporary jet velocity profiles at the collar exit cross-section were also determined. These profiles are shown in Fig. 9. A $T/4$ phase shift between the velocity and jet diameter is clearly visible. It follows

from Fig. 9 that in this oscillation phase in which the flow velocity in the axis reaches its extreme values, the jet diameter is approximately the same as the duct diameter. However in the stages in which the flow velocity in the axis is close to the mean value, the jet diameter takes an extreme value.

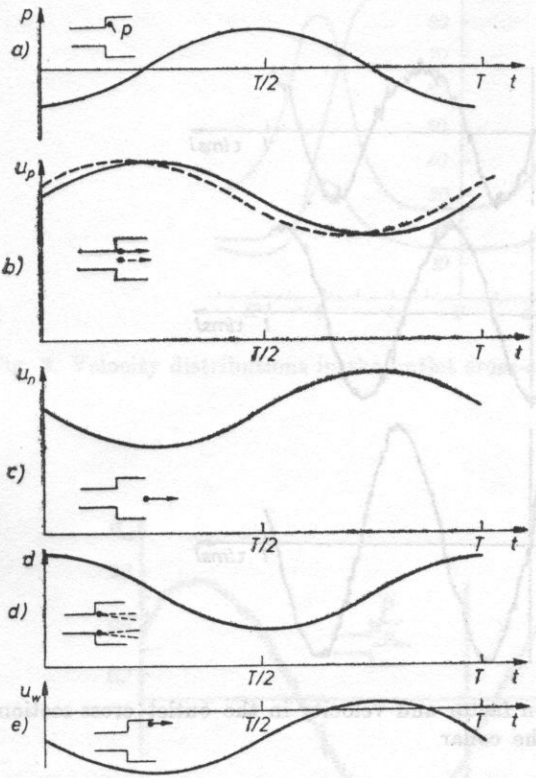

Fig. 8. Traces of the basic flow properties of the jet
a) pressure p; b) velocity at the duct outlet, u_p; c) velocity at the collar outlet u_n; d) jet diameter d; e) velocity at the wall, u_w

Table 1. Phase shifts of flow velocity traces with respect to the pressure trace

Duct outlet	jet axis	$^5/_8T$
	jet boundary	$^3/_4T$
Collar outlet	jet axis	$^1/_4T$
	jet boundary	$^1/_2T$
	wall	$^1/_4T$

Fig. 10 shows a set of correlation functions for points along the axis of the jet. In Fig. 11 the phases with zero value of the correlation functions are arranged versus the position of the thermoanemometer probe. The inclination of a line represents the phase velocity. It follows from Fig. 11 that beyond the flow region close to the outlet of the duct the phase velocity is constant (50 m/s).

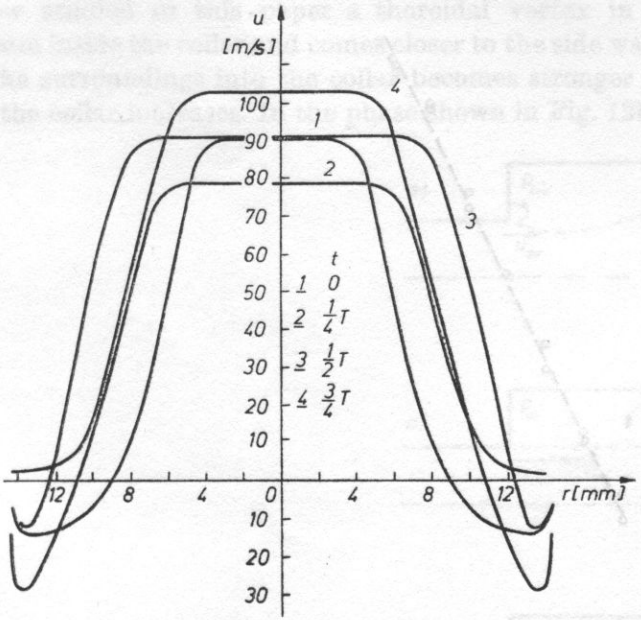

Fig. 9. Temporary profiles of the velocity in the collar outlet
r – the distance from the collar axis

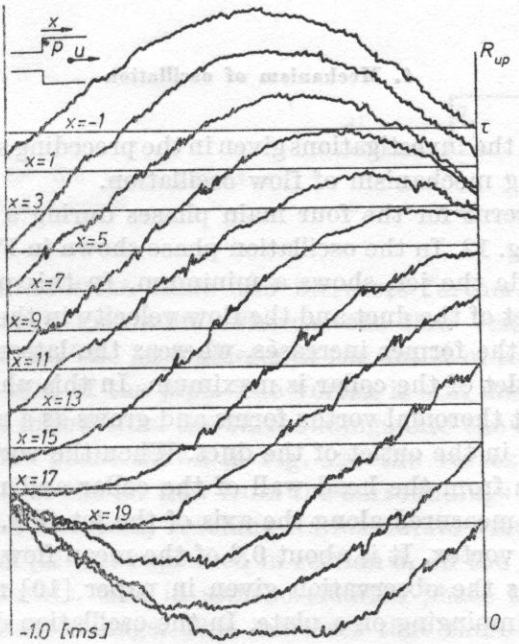

Fig. 10. Set of correlograms for different positions of the thermoanemometer probe along the collar axis

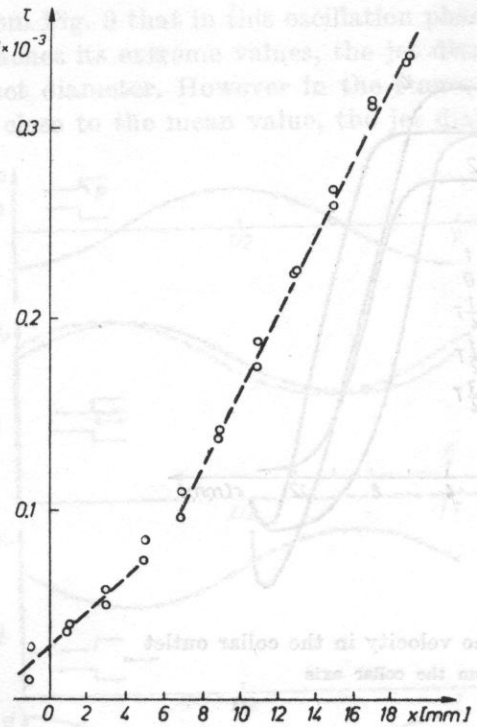

Fig. 11. Positions of the phase surface for zero value of the correlation functions given in Fig. 10

4. Mechanism of oscillation

The results of the investigations given in the preceding sections of this paper justify the following mechanism of flow oscillation.

The flow patterns for the four main phases during a cycle of oscillation are illustrated in Fig. 12. In the oscillation phase shown in Fig. 12a the pressure in the collar, outside the jet, shows a minimum. In this phase both the flow velocity in the outlet of the duct and the flow velocity in the outlet of the collar take mean values; the former increases, whereas the latter decreases. The jet diameter at the outlet of the collar is maximum. In this phase, or in a slightly ealier one, a distinct thoroidal vortex forms and grows as a result of an increase in the flow velocity in the outlet of the duct. When the vortex becomes strong enough it separates from the head wall of the collar and moves downstream. The phase velocity measured along the axis of the jet (Fig. 11) corresponds to the velocity of this vortex. It is about 0.6 of the mean flow velocity of the jet. This result confirms the observation given in paper [10] regarding the oscillation of a free jet impinging on a plate. In the oscillation discussed in [10] an important role is played by coherent vortices forming from smaller ones in the process of the so-called "collective interaction".

In the flow studied in this paper a thoroidal vortex in creases as it moves downstream inside the collar and comes closer to the side wall. As a result, the flow from the surroundings into the collar becomes stronger and therefore the pressure in the collar increases. In the phase shown in Fig. 12b the pressure

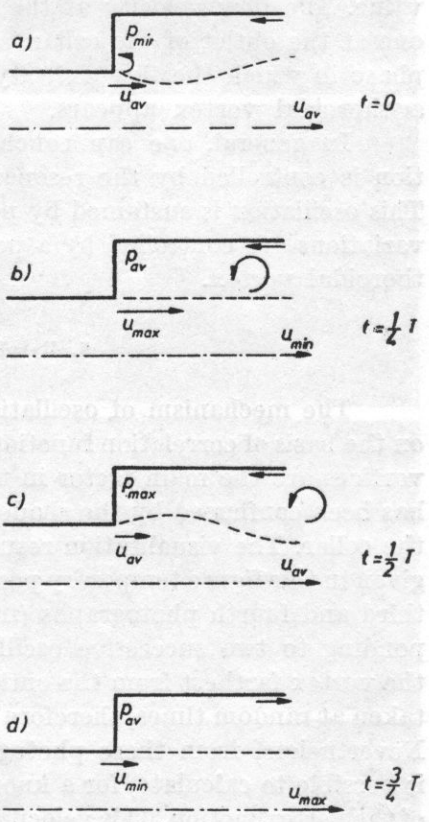

Fig. 12. Flow patterns for the main phases of the oscillation cycle

in the collar reaches the mean value and increases further. The flow velocity in the outlet of duct is maximum, whereas the flow velocity in the outlet of the collar is minimum. The jet diameter at the outlet of the collar is approximately the same as that of the pipe. The vortex is still inside the collar close to the outlet and the inflow from the surroundings into the collar is maximum.

In the successive phase shown in Fig. 12c the vortex is already outside the collar. As a result of the air flow from the surroundings into the collar, the pressure in the collar increases, reaching its maximum value higher than the surrounding pressure. (It was explained in section 3, on the basis of the results of velocity measurements, that in some oscillation phase the air flows along the walls into the surroundings. This indicates that there is overpressure in the collar). The flow velocities in the outlet of the duct and the outlet of the collar take mean values; the former decreases, whereas the latter increases.

The jet diameter at the outlet of the collar reaches its maximum value. In the further oscillation phase the pressure in the collar decreases as a result of the air outflow (along the walls) and of the jet ejection.

In the phase shown in Fig. 12 d the pressure in the collar has its mean value. The flow velocity at the outlet of the duct is minimum, whereas the one at the outlet of the collar is maximum. It is possible that already in this phase in which the flow velocity at the outlet of the duct starts to increase, a thoroidal vortex appears.

In general, one can conclude that the oscillation mechanism in question is controlled by the resonance oscillation of an air column in the duct. This oscillation is sustained by periodic pressure variations in the collar. These variations are controlled by a periodically appearing and downstream moving thoroidal vortex.

5. Results of flow visualisation

The mechanism of oscillation described above has been deduced mainly on the basis of correlation functions and velocity measurements. Strong thoroidal vortices are the main factor in this mechanism. The existence of the vortices has been confirmed by the shadow graph visualisation of a free stream outside the collar. The visualisation results are shown in Fig. 13. In the photographs given in this figure temporary positions of this vortex can be seen. In the second, third and fourth photographs (from top) one can observe two vortices corresponding to two successive oscillation cycles. As a result of flow turbulence, the vortex farthest from the outlet is partly distorted. These photographs were taken at random times, therefore the time intervals between them are unknown. Nevertheless, from these photographs in which two vortices can be seen, it is possible to calculate, for a known pulsation period, the approximate velocity of the vortex motion. This velocity is about 50 m/s and agrees with the previously calculated phase velocity.

6. Conclusions

The investigations reported on in this paper have confirmed the existence of strong oscillations in subsonic flow in a duct with a sudden cross-section increase. These oscillations are the source of an acoustic wave which increases the overall sound level generated by a jet by about 30 dB. The oscillation mechanism is controlled by the resonance oscillation of an air column in the duct. This oscillation is sustained by flow in the collar. These oscillations occur over a relatively wide range of variations in the flow velocity and collar length. One can suppose that the oscillation mechanism described above is not the only one. Preliminary investigations have shown some different flow patterns for higher flow velocities, which are now studied.

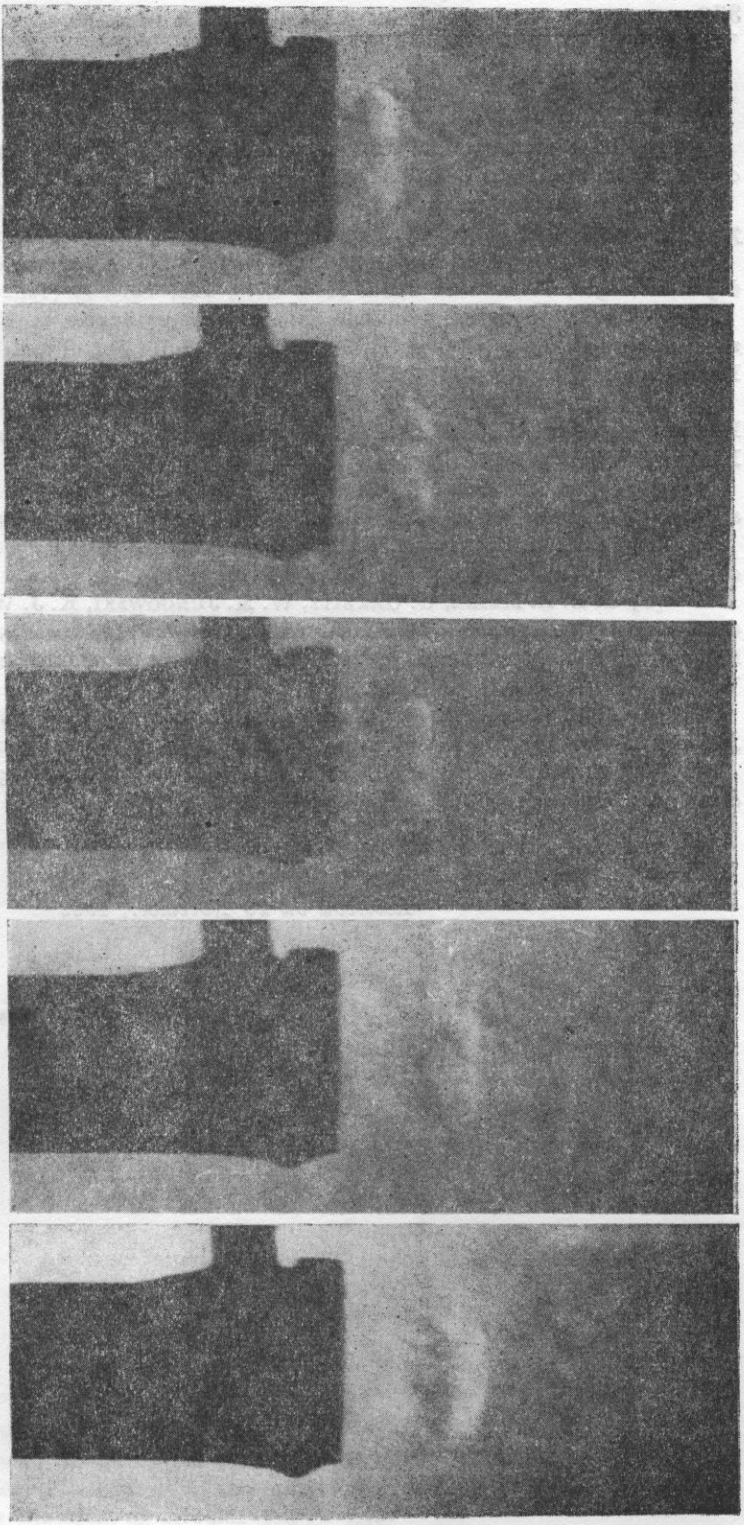

Fig. 13. Photographs of the shadow graph visualisation of the free jet

References

[1] D. ROCKWELL, E. NAUDASHER, *Review: Self-sustaining oscillations of flow past cavities*, Journal of Fluid Engineering (Trans. ASME), **100**, 2, 152-165 (1978).

[2] D. ROCKWELL, A. SCHACHENMANN, *Self-generation of organized waves in an impinging turbulent jet at low Mach number*, Journal of Fluid Mechanics, **117**, 425-441 (1982).

[3] C. KNISELY, D. ROCKWELL, *Self-sustained low-frequency components in an impinging shear layer*, Journal of Fluid Mechanics, **116**, 157-186 (1982).

[4] A. G. STRUYT, *Flow-induced acoustic resonances in ducts with flow-measuring nozzles having a recess*, Euromech 34 Colloquium on Control and Feedback Mechanisms in Flow Noise, Göttingen 1972.

[5] R. RAMAKRISHNAN, P. O. A. L. DAVIS, *Sound generation by flow-acoustic coupling*, Proceedings of the JUTAM/JCA/AIAA Symposium on Mechanics of Sound Generation in Flows, Göttingen 1979, Springer Verlag, pp. 62-68.

[6] W. G. Jr. HILL, R. R. GRENE, *Increased turbulent jet mixing rates obtained by self-excited acoustic oscillations*, Journal of Fluid Engineering (Trasn. ASME) (Sept. 1977).

[7] M. A. Z. HASAN, A. K. M. F. HUSSAIN, *A formula for resonance frequencies of a whistler nozzle*, J. Acoust. Soc. Am., 65 (May 1979).

[8] G. E. A. MEIER, G. GRABITZ, W. M. JUNGOWSKI, K. J. WITCZAK, J. S. ANDERSON, *Oscillations of the supersonic flow downstream of an abrupt increase in duct cross-section*, Mitteilungen aus dem Max-Planck-Institut für Strömungsforschung und der Aerodynamischen Versuchsanstalt, Göttingen 1978.

[9] A. P. SZUMOWSKI, G. E. A. MEIER, *Schwingungen der Überschallströmung in einem Kanal mit Querschnittssprung*, Max-Planck-Institut für Strömungsforschung, Bericht 23, 1978.

[10] CHIN-MING HO, N. S. NOSSEIR, *Dynamics of an impinging jet, part 1. The feed back phenomenon, part 2. The noise generation*, Journal of Fluid Mechanics, **105**, 119-142 (1981); **116**, 379-391 (1982).

Received on 29 November, 1982

ARCHIVES OF ACOUSTICS
3, 4, 331-340 (1983)

THE SOUND POWER OF A CIRCULAR PLATE FOR HIGH-FREQUENCY WAVE RADIATION

WITOLD RDZANEK

Pedagogical University (65-069 Zielona Góra, Plac Słowiański 6)

This paper gives an analysis of the sound power of a circular plate which vibrates at a frequency much higher than the resonance one. This analysis was carried out for Bessel axially-symmetric distributions of vibration velocity on the surface of a source placed in a rigid, planar baffle. An exact expression of the sound power of the vibrating circular plate was given in Hankel representation. It was assumed in a specific case that the source radiated waves at frequencies much higher than the resonance ones, permitting simplifications to be introduced in the subintegral function. As the final result of the analysis, an approximate expression was derived using the Cauchy theorem on residua. The expressions derived here are very useful and convenient for numerical calculations.

Notation

a — plate radius
c_o — sound wave propagation velocity in a medium of density ϱ_0
$H_n^{(1)}(x)$ — Hankel function of the nth order of the first kind
$H_n^{(2)}(x)$ — Hankel function of the nth order of the second kind
$I_n(x)$ — modified Bessel function of the nth order of the first kind
$J_n(x)$ — Bessel function of the nth order
k — wave number
$K_n(x)$ — cylindrical MacDonald function of the nth order
N — real component of source acoustic power (A2), (A3)
N_0 — real power of source for $k \to \infty$ (A10)
p — sound pressure (A1)
r — radial variable
v — vibration velocity amplitude of source surface points
v_n — vibration velocity amplitude of source points of the plate (1)
v'_{0n} — vibration velocity amplitude of the central point of the plate
W — characteristic function of circular source (A8)

W_n — characteristic function of circular plate for (0, n) vibration mode (4)
$Z_n(x)$ — cylindrical function of the nth order
λ — sound wave length
ϱ_0 — density of gaseous medium
σ — source surface area
ω — angular frequency

1. Introduction

The problem of the impendance and sound power of circular sources with an irregular vibration velocity distribution has been the object of analysis in a large number of papers in the field of acoustic wave generation by surface sources. In terms of subject papers [3-8] are above all most related to the problems considered in the present paper (a full bibliography of this problem was given in paper [3]). Most of the investigation results obtained could be used in partical applications only when using computers. Of the results obtained, only the expressions of impedance and sound power appeared to be convenient in a small number of cases, above all and most frequently for very small interference parameters.

These have been to date a lack of elaborations giving the form of the expressions of the sound power of a circular plate in a speciafic case which would be convenient for numerical calculations, namely for high-frequency wave radiation. The investigations reported on in the present paper have given such relationships.

The present considerations of the radiation of a circular plate refer to the results obtained in paper [6], where the object of investigation also included the problem of the sound power of a circular membrane for frequencies much higher than the resonance ones.

In terms of the possibility of practical applications, analysis was carried out on the axially-symmetric vibration of a circular plate clamped on the circumference to an ideal rigid and planar baffle. Linear processes harmonic in time were considered.

Taking as the basis the Huygens-Rayleigh integral formula, exact expressions were introduced for sound power in the form of a single integral. It was assumed in a specific case that the plate radiated waves at frequencies much higher than the resonance ones. This permitted simplifications in the subintegral function and subsequently integration using the Cauchy residua theorem.

Very useful and convenient expressions were derived for numerical calculations.

2. Exact calculation of the sound power

In considering the linear phenomena sinusoidally dependent on time, the axially – symmetric proper vibration of a circular plate clamped on the

circumference can be described in the following way [8]:

$$v_n(r) = v_{0n}\left\{J_0(r\beta_n) - \frac{J_0(a\beta_n)}{J_0(ia\beta_n)} J_0(ir\beta_n)\right\}, \tag{1}$$

where a is the radius of the plate, v_{0n} is the vibration velocity amplitude of points of the plate, r is a radial variable, J_0 is a Bessel function of *zero*th order and $a\beta_n$ is the nth root of the equation

$$J_0(a\beta_n)I_1(a\beta_n) = -J_1(a\beta_n)I_0(a\beta_n), \tag{2}$$

where I_s is a modified Bessel function of the sth order. The constant v_{0n} can be expressed by the vibration velocity of the central point of the plate v'_{0n}, from the following relation

$$v'_{0n} = v_{0n}\left[1 - \frac{J_0(a\beta_n)}{J_0(ia\beta_n)}\right]. \tag{2a}$$

The expression of the vibration velocity (1) can be inserted into relationship (A8) and the following integral property [9] used:

$$\int_0^u wJ_0(hw)J_0(lw)\,dw = \frac{u}{h^2 - l^2}\{hJ_1(hu)J_0(lu) - lJ_0(hu)J_1(lu)\}, \tag{3}$$

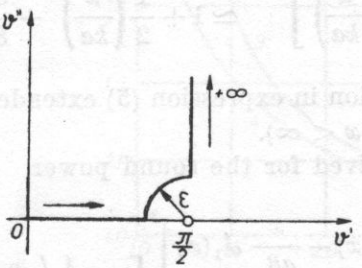

Fig. 1. Integration in the plane of the complex variable $\vartheta = \vartheta' + i\vartheta''$ for expression (A4), $\varepsilon \to 0$

as a result of which the characteristic function $W_n(\vartheta)$ of the circular plate for a (0, n) vibration mode is

$$W_n(\vartheta) = v_{0n}\frac{2\beta_n^2}{\beta_n^4 - k^4\sin^4\vartheta}\{a\beta_n J_1(a\beta_n)J_0(ka\sin\vartheta) - ka\sin\vartheta J_0(a\beta_n)J_1(ka\sin\vartheta)\}. \tag{4}$$

The real power radiated by the circular plate by the (0, n) vibration mode can be calculated from relationship (A9). This involves the substitution

$x = ka\sin\vartheta$, giving

$$N_n = 4(a\beta_n)^6 N_0 \int_0^{ka} \left\{ \frac{a_n J_0(x) - \dfrac{x}{a\beta_n} J_1(x)}{(a\beta_n)^4 - x^4} \right\}^2 \frac{x\,dx}{\sqrt{1-(x/ka)^2}}, \tag{5}$$

where

$$a_n = \frac{J_1(a\beta_n)}{J_0(a\beta_n)}; \tag{6}$$

whereas

$$N_0 = \varrho_0 c_0 \pi a^2 v_{0n}^2 J_0^2(a\beta_n) \tag{7}$$

is an expression of the sound power radiated by a circular plate by the $(0, n)$ vibration mode in the case when $k \to \infty$ (see relationship (A11)), with $k = \omega/c_0$, where ω is the angular frequency and c_0 is the sound wave propagation velocity in a medium of density ϱ_0.

3. Approximate calculation of the sound power

In a specific case, when the wave radiation frequency is much higher than the resonance frequency ($k \gg \beta_n$), the approximate formula

$$\left[1-\left(\frac{x}{ka}\right)^2\right]^{-1/2} \simeq 1 + \frac{1}{2}\left(\frac{x}{ka}\right)^2 + \frac{3}{8}\left(\frac{x}{ka}\right)^4 \tag{8}$$

can be used and integration in expression (5) extended from finite ($0 \leqslant x \leqslant ka$) to infinite limits ($0 \leqslant x < \infty$).

The expression derived for the sound power

$$N_n = 4(a\beta_n)^6 N_0 \int_0^{\infty} \left\{ \frac{a_n J_0(x) - \dfrac{x}{a\beta_n} J_1(x)}{(a\beta_n)^4 - x^4} \right\}^2 \left[1 + \frac{1}{2}\left(\frac{x}{ka}\right)^2 + \frac{3}{8}\left(\frac{x}{ka}\right)^4\right] x\,dx \tag{9}$$

can be given in the form of an integral sum calculated from the integral formula (A14).

For the first derivatives of the special functions the following relations can be used [9]:

$$\begin{aligned} J_0'(x) &= -J_1(x), & xJ_1'(x) &= xJ_0(x) - J_1(x), \\ H_0^{(1)\prime}(x) &= -H_1^{(1)}(x), & xH_1^{(1)\prime}(x) &= xH_0^{(1)}(x) - H_1^{(1)}(x), \\ I_0'(x) &= I_1(x), & xI_1'(x) &= xI_0(x) - I_1(x), \\ K_0'(x) &= -K_1(x), & xK_1'(x) &= -xK_0(x) - K_1(x), \end{aligned} \tag{10}$$

where $H_0^{(1)}(x)$ and $H_1^{(1)}(x)$ are Hankel functions of the first kind, whereas $K_0(x)$ and $K_1(x)$ are cylindrical MacDonald functions, both pairs being respectively of the *zero*th and first orders.

When in addition the characteristic equation (2), determination (6) and the wronskians [9]

$$H_0^{(1)}(x)J_1(x) - J_0(x)H_1^{(1)}(x) = \frac{2i}{\pi x},$$
$$K_0(x)I_1(x) + I_0(x)K_1(x) = \frac{1}{x}, \tag{11}$$

are taken into consideration, finally thus

$$N_n = N_0 \left\{1 + \frac{1}{2}\alpha_n^2 \frac{(a\beta_n)^2}{(ka)^2} - \frac{3}{4}\alpha_n \frac{(a\beta_n)^3}{(ka)^4}\right\}, \tag{12}$$

if $k \gg \beta_n$.

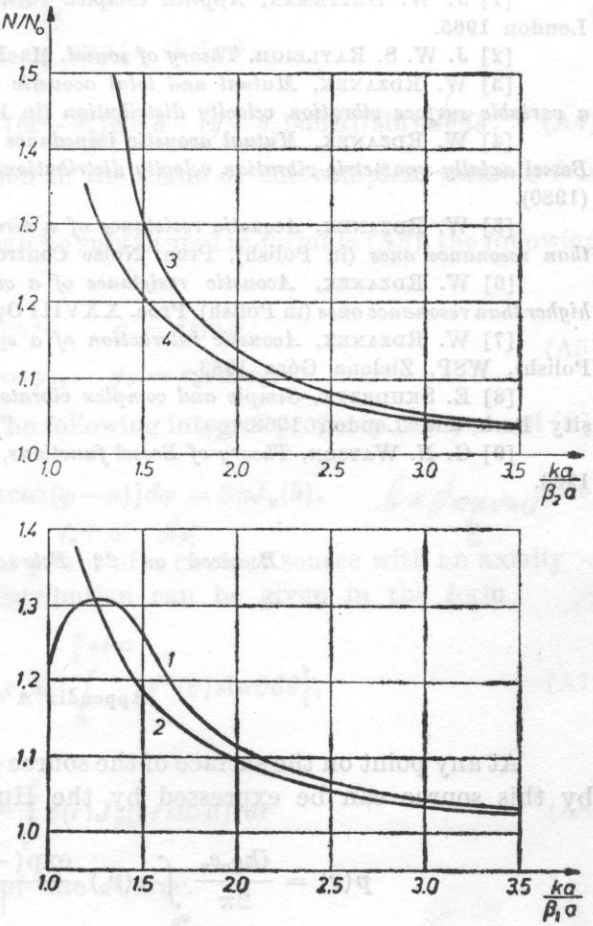

Fig. 2. The relative sound power N/N_0 of the circular plate for (0, 1) and (0, 2) axially-symmetic vibration modes, depending on $ka/\beta_n a$

Curves 1 and 3 have been plotted from the exact formula (5); curves 2 and 4, from the approximate formula (12). It is assumed that $\beta_1 a = 3.195$ and $\beta_2 a = 6.306$

4. Conclusions

The approximate expression (12) derived is very convenient for numerical calculations of the sound power radiated by a circular plate with axially-symmetric vibration modes and can be used with less demanding assumptions than $ka \gg a\beta_n$. E.g. with $ka > 3a\beta_n$ the sound power for the first few vibration modes involves relative error not exceeding 1 per cent (Fig. 2).

In a boundary case, for $ka \to \infty$, it can be shown from formula (12) that the relative sound power N/N_0 tends to unity.

When $ka < 3a\beta_n$, or when high accuracy is required of results, calculations can be carried out by computers from the integral formula (5).

References

[1] J. W. DETTEMAN, *Applied complex variables*, McMillan Company, New York London 1965.

[2] J. W. S. RAYLEIGH, *Theory of sound*, MacMillan, London 1929.

[3] W. RDZANEK, *Mutual and total acoustic impedance of a system of sources with a variable surface vibration velocity distribution* (in Polish), WSP, Zielona Góra 1979.

[4] W. RDZANEK, *Mutual acoustic impedance of circular membranes and plates with Bessel axially-symmetric vibration velocity distributions*, Archives of Acoustics, **5**, 3, 237-250 (1980).

[5] W. RDZANEK, *Acoustic resistance of a circular plate for frequencies much higher than resonance ones* (in Polish), Proc. Noise Control 82, Cracow 1982.

[6] W. RDZANEK, *Acoustic resistance of a circular membrane for frequencies much higher than resonance ones* (in Polish). Proc. XXVIII Open Seminar on Acoustics, Gliwice 1981.

[7] W. RDZANEK, *Acoustic interaction of a system of concentric annular sources* (in Polish), WSP, Zielona Góra 1983.

[8] E. SKUDRZYK, *Simple and complex vibratory systems*, University Press, University Park and London 1968.

[9] G. N. WATSON, *Theory of Bessel functions*, 2nd ed., University Press, Cambridge 1966.

Received on 22 February, 1983

Appendix A

At any point on the surface of the source the sound pressure $p(\boldsymbol{r})$ generated by this source can be expressed by the Huygens-Rayleigh formula [2]

$$p(\boldsymbol{r}) = \frac{ik\varrho_0 c_0}{2\pi} \int_{\sigma_0} v(\boldsymbol{r}_0) \frac{\exp(-ik|\boldsymbol{r}-\boldsymbol{r}_0|)}{|\boldsymbol{r}-\boldsymbol{r}_0|} d\sigma_0, \tag{A1}$$

where $|\boldsymbol{r}-\boldsymbol{r}_0| = \sqrt{(x-x_0)^2+(y-y_0)^2}$ is the distance between any two points on the surface of the source, c_0 is the sound wave propagation velocity in a medium of density ϱ_0, $k = 2\pi/\lambda$ is a wave number and λ is wavelength.

The real component of the sound power emitted by the source is

$$N = \frac{1}{2}\,\mathrm{Re}\left\{\int_\sigma p(\boldsymbol{r})\,v(\boldsymbol{r})\,d\sigma, \right. \tag{A2}$$

or, considering relation (A1),

$$N = \mathrm{Re}\left\{\frac{ik\varrho_0 c_0}{4\pi}\int_\sigma\int_{\sigma_0} v(\boldsymbol{r})\,v(\boldsymbol{r}_0)\,\frac{\exp(-ik|\boldsymbol{r}-\boldsymbol{r}_0|)}{|\boldsymbol{r}-\boldsymbol{r}_0|}\,d\sigma_0 d\sigma\right\}. \tag{A3}$$

This formula represents the real power emitted by the source into the surrounding space, i.e. the energy flux radiated by the source over one full period.

The surface integrals in formula (A3) can be calculated using the following expansion [3], [7],

$$\frac{\exp(-ik|\boldsymbol{r}-\boldsymbol{r}_0|)}{|\boldsymbol{r}-\boldsymbol{r}_0|} = -\frac{ik}{2\pi}\int_0^{\frac{\pi}{2}+i\cdot\infty}\int_0^{2\pi}\exp\{-ik\sin\vartheta\times$$
$$\times[(x-x_0)\cos\alpha+(y-y_0)\sin\alpha]\}\sin\vartheta\,d\vartheta\,d\alpha. \tag{A4}$$

The course of the integration in the plane of the complex variable ϑ is given in Fig. 1 (see p. 333).

The integral function (A4) can be substituted in formula (A3), the following polar coordinates introduced:

$$\begin{aligned} x &= r\cos\varphi, \quad & y &= r\sin\varphi, \\ x_0 &= r_0\cos\varphi_0, \quad & y_0 &= r_0\sin\varphi_0, \end{aligned} \tag{A5}$$

changing the integration order. The following integral property can be used [9]:

$$\int_0^{2\pi}\exp[\pm ib\cos(\varphi-a)]\,d\varphi = 2\pi J_0(b). \tag{A6}$$

The expression of the sound power of a circular source with an axially — symmetric vibration velocity distribution can be given in the form

$$N = \mathrm{Re}\left\{\varrho_0 c_0 \pi k^2 \int_0^{\frac{\pi}{2}+i\cdot\infty} W^2(\vartheta)\sin\vartheta\,d\vartheta\right\}, \tag{A7}$$

where

$$W(\vartheta) = \int_0^a v(r)\,J_0(kr\sin\vartheta)\,r\,dr \tag{A8}$$

is the characteristic function of the source.

The real component of sound power, i.e. the real power, can be determined from expression (A7) when the integration in the plane of the complex variable is carried out over a section on the real axis ϑ in the limits $(0, \pi/2)$, i.e.

$$N = \varrho_0 c_0 \pi k^2 \int_0^{\pi/2} W^2(\vartheta) \sin\vartheta d\vartheta. \tag{A9}$$

In numerical calculations it is convenient to use the concept of relative sound power N/N_0, where N_0 can be assumed to be the real power of the source for $k \to \infty$. When $k \to \infty$, $p(\boldsymbol{r}) = \varrho_0 c_0 v(\boldsymbol{r})$, and then, according to formula (A2),

$$N_0 = \lim_{k\to\infty} N = \frac{1}{2} \varrho_0 c_0 \int_\sigma v^2(\boldsymbol{r}) d\sigma. \tag{A10}$$

When the sound source is circular and the vibration velocity distribution axially — symmetric,

$$N_0 = \pi \varrho_0 c_0 \int_0^a v^2(r) r dr, \tag{A11}$$

where a is the radius of the circular plate.

Appendix B

The contour integral (see [9])

$$\frac{1}{2\pi i} \int_C z^{\varrho-1} Z_\mu(bz) \frac{H_\nu^{(1)}(az)\, dz}{(z^4 - r^4)^2}, \tag{A12}$$

where $a > b > 0$, r is a complex number, Z_μ is a cylindrical function of the order μ, $|\mu| + |\nu| < \varrho < 10$, can be expressed in the form of the sum of the residua at the poles of the subintegral function. When $a = b$, then $\varrho < 9$.

Using the Jordan lemma and Cauchy's residua theorem [1] the integration contour C can be closed in the upper half-plane of the complex variable z. This integration covers the two poles of the subintegral function for $z = r$ and $z = ir$. This gives

$$\frac{1}{2\pi i} \int_0^\infty \{Z_\mu(bx) H_\nu^{(1)}(ax) - \exp(\varrho\pi i) Z_\mu[bx\exp(\pi i)] \times$$

$$\times H_\nu^{(1)}[ax\exp(\pi i)]\} \frac{x^{\varrho-1} dx}{(x^4 - r^4)^2} = \frac{1}{16 r^3} \frac{d}{dr} \{r^{\varrho-4} [Z_\mu(br) H_\nu^{(1)}(ar) +$$

$$+ i^{\varrho-4} Z_\mu(ibr) H_\nu^{(1)}(iar)]\}. \tag{A13}$$

In a specific case for $Z_\mu = J_\mu$, $a = b = 1$, considering the relationships

$$J_\mu(ir) = \exp\left(i\mu\frac{\pi}{2}\right) I_\mu(r),\ H_\nu^{(1)}(ir) = \frac{2}{\pi}\exp\left[-i(\nu+1)\frac{\pi}{2}\right]K_\nu(r),$$

$$J_\mu(-x) = \exp(\mu\pi i)J_\mu(x), \qquad H_\nu^{(1)}(-x) = -\exp(-i\nu\pi)H_\nu^2(x),$$

(A13) becomes

$$\int_0^\infty J_\mu(x)J_\nu(x)\frac{x^{\varrho-1}dx}{(x^4-r^4)^2} = \frac{1}{8r^3}\frac{d}{dr}\left\{r^{\varrho-4}\left[\frac{\pi i}{2}J_\mu(r)H_\nu^{(1)}(r) + \right.\right.$$

$$\left.\left. + \exp\left[i(\varrho+\mu-\nu)\frac{\pi}{2}\right] I_\mu(r)K_\nu(r)\right]\right\}, \quad \text{(A14)}$$

when $|\mu| + |\nu| < \varrho < 9$.

ARCHIVES OF ACOUSTICS
8, 4, 341-354 (1983)

THE APPLICATION OF FOURIER INTEGRAL TRANSFORMS IN A GENERAL THEORY OF DIFFRACTION

ROMAN WYRZYKOWSKI

WSP (35-311 Rzeszów, ul. Rejtana 16a)

Integral transforms have frequently been used to solve different specific problems in diffraction. There has, however, been no application of this method to the fundamental equations of diffraction theory.

The present author shows that a transition from the d'Alambert equation to the Helmholtz equation for transforms gives all pulse fields, i.e. the acoustic potential of this field as the inverse transform of the product of the transform of the time behaviour of the pulse and the potential for a harmonic wave. This method permits relatively easy calculations of the sound pulse fields, with the additional assumption that the pulse distribution on the source can be represented as the product of a position-dependent function and one which is time-dependent.

1. Introduction

It is now generally known that the use of integral transformation for arbitrary (nonharmonic) time behaviour facilitates to a large extent the solution of diffraction problems. Papers [4, 5, 7-12, 15] in which different integral transformations were used in the problems of pulse diffraction at wedges or half-planes are now classical. It was found in [6] that a Fourier integral transform changes the d'Alambert equation into the Helmholtz one and the authors were thus able to calculate the field of a pulse-excited point source.

To date, however, there has been no general formulation of this problem, i.e. the use of integral transformation in the fundamental, general problems of diffraction theory. It is to these problems that the present paper is devoted.

It is assumed that all pulses considered below do not exceed the conditions set in linear acoustics. The theory of nonlinear pulses requires a completely different approach, while this subject would go far beyond the framework of the present paper.

It is also assumed that the pulse which excites the sound source can be given in the form of the product of a function dependent on spatial variables and a function dependent on time.

2. Theory

The so-called general theory of harmonic wave diffraction is concerned with the solution of the Helmholtz equation with definite boundary conditions

$$\Delta\varphi + k^2\varphi = 0, \tag{1.1}$$

where φ is the acoustic potential and k is a wave number. In this case the time dependence factor $\exp(\pm i\omega t)$ is neglected and the acoustic potential regarded as a function of position, which can symbolically be given as

$$\varphi = \varphi(x_i), \quad i = 1, 2, 3. \tag{1.2}$$

Naturally, the physical phenomenon in the acoustic field is, according to the accepted convention, represented by one of the products

$$\varphi(x_i)\exp(i\omega t), \quad \varphi(x_i)\exp(-i\omega t). \tag{1.3}$$

Equation (1.1) is solved in volume area V limited by a closed surface S on which sound sources are distributed. The sources show the vibration amplitude

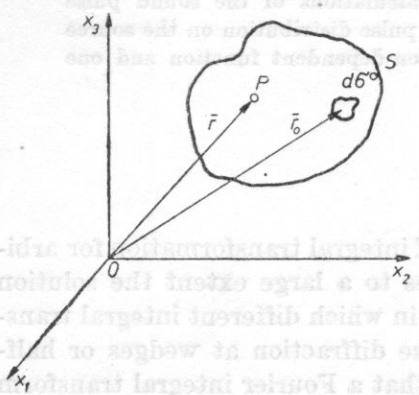

Fig. 1. The geometry of the radiating system

distribution $u_0(x_i)$, where, according to the definition of acoustic potential, φ,

$$u_0(x_i) = -\left(\frac{\partial\varphi}{\partial n}\right)_{S_0}, \tag{1.4}$$

which is shown in Fig. 1. Although the basic literature [13], [16] gives the so-called Poisson's integral formula which generalizes harmonic wave theory to arbitrary time behaviour, but this formula is very complicated and no known achievements in pulse diffraction theory have been based on it.

The present paper is concerned with nonharmonic processes; it is assumed that the acoustic potential is a function of position and time:

$$\varphi = \varphi(x_i, t), \tag{1.5}$$

i.e. it satisfies the d'Alambert wave function

$$\Delta\varphi - \frac{1}{c^2}\frac{\partial^2\varphi}{\partial t^2} = 0 \tag{1.6}$$

in the volume V with the boundary conditions given above. In order to carry out Fourier integral transformation, the transform of the acoustic potential (1.5) should first be written in the form [1]

$$\Phi(x_i, \omega) = \frac{1}{\sqrt{2\pi}} \int_{-\infty}^{\infty} \varphi(x_i, t)\exp(-i\omega t)\,dt. \tag{1.7}$$

Consideration that [1]

$$\frac{\partial^2\varphi}{\partial t^2} \rightarrow i^2\omega^2\varphi \tag{1.8}$$

gives from (1.6) the transform equation in the form

$$\Delta\Phi + \frac{\omega^2}{c^2}\Phi = 0, \tag{1.9}$$

i.e.

$$\Delta\Phi + k^2\Phi = 0. \tag{1.10}$$

(1.10) is a Helmholtz equation, but the transform $\Phi(x_i)$ must satisfy also those conditions which are set in the classical theory of harmonic waves for the potential itself. As it was mentioned in the **Introduction**, the authors of paper [6] took as the basis the fact that the acoustic potential transform satisfies the Helmholtz equation and used it in the case of a pulse-excited point source. In the present paper this problem will be considered in most general terms. Since the solution of the Helmholtz equation consists in differential and integral operations on Φ with respect to spatial variables, all solutions of the Helmholtz equation, i.e. for the harmonic wave potential, give simultaneously the expression of the Fourier transform of the potential of an arbitrary time pulse.

It can now be considered how the above statement, whose form does not seem so far to be precise enough, can be used in practice.

In the problems related to wave diffraction the following procedure can be used: the same Green function as that for harmonic waves [13], [16] is introduced for the transform $\Phi(x_i, \omega)$:

$$\Phi(x_i, \omega) = \int_S \left[G(x_i, x_i^0)\frac{\partial\Phi(x_i^0)}{\partial n} - \Phi(x_i^0)\frac{\partial G(x_i, x_i^0)}{\partial n}\right] d\sigma^0, \tag{1.11}$$

and in the case of the so-called acoustic Green function [16] satisfying the condition

$$\frac{\partial G}{\partial n} = 0 \quad \text{on the surface } S \tag{1.12}$$

this gives finally

$$\Phi(x_i, \omega) = \int_S G(x_i, x_i^0) \frac{\partial \Phi(x_i^0)}{\partial n} d\sigma^0. \tag{1.13}$$

In order to prevent their form becoming too complicated, in the above fomulae the obvious dependence on ω was not given under the integral. The symbol o refers to the sound source.

The derivative $\partial\Phi/\partial n$ can now be interpreted on the surface of the sound source. From the transformation formula (1.17)

$$\frac{\partial \Phi}{\partial n} = \frac{\partial}{\partial n} \int_{-\infty}^{\infty} \varphi(x_i, t) \exp(-i\omega t) dt = \int_{-\infty}^{\infty} \frac{\partial \varphi(x_i, t)}{\partial n} \exp(-i\omega t) dt, \tag{1.14}$$

and from the definition of the acoustic potential (1.4)

$$\frac{\partial \Phi}{\partial n} = -\int_{-\infty}^{\infty} u_0(x_i, t) \exp(-i\omega t) dt = -U_0(x_i, \omega). \tag{1.15}$$

It can be seen that the derivative $\partial\Phi/\partial n$ represents the Fourier transform of the vibration velocity on the sound source. It should be stressed that in this case $u_0(x_i, t)$ does not denote the vibration velocity amplitude but the time behaviour of the pulse velocity, which in a general case is also a function of position. Since the direction outside from the volume V is taken as the positive direction of the normal and the opposite direction as the positve direction of the vibration velocity, from formula (1.15), (1.13) can now be written as

$$\Phi(x_i, \omega) = \int_S G(x_i, x_i^0) U_0(x_i^0, \omega) d\sigma^0. \tag{1.16}$$

Particularly for a half-space bounded by a rigid plane on which the sound sources lie, using the notation from Fig. 1, the Green function can be given in the form

$$G(\boldsymbol{r}, \boldsymbol{r}_0) = \frac{1}{2\pi} \frac{\exp(ik|\boldsymbol{r} - \boldsymbol{r}_0|)}{|\boldsymbol{r} - \boldsymbol{r}_0|}. \tag{1.17}$$

Formula (1.16) which represents the acoustic potential tranform as a function of position and the angular frequency ω now becomes

$$\Phi(\boldsymbol{r}, \omega) = \frac{1}{2\pi} \int_{S^0} \frac{\exp(ik|\boldsymbol{r} - \boldsymbol{r}_0|)}{|\boldsymbol{r} - \boldsymbol{r}_0|} U_0(\boldsymbol{r}_0, \omega) d\sigma^0. \tag{1.18}$$

In practical cases it is almost always possible to represent the pulse velocity distribution as the product of the position and time functions, i.e. to assume that all points of the source are excited by the same time behaviour. In such a case

$$u_0(x_i^0, t) = u_0(x_i^0) f(t). \tag{1.19}$$

Using the Fourier transform (1.15) in $u_0(x_i, t)$ only the time function $f(t)$ is transformed, i.e.

$$\frac{\partial \Phi}{\partial n} = -u_0(x_i) \int_{-\infty}^{\infty} f(t) \exp(-i\omega t)\, dt = -u_0(x_i^0) F(\omega), \tag{1.20}$$

where $F(\omega)$ is the transform of the function representing the time behaviou of the pulse $f(t)$. Therefore, using the notation from Fig. 1,

$$U_0(\boldsymbol{r}_0, \omega) = u_0(\boldsymbol{r}_0) F(\omega). \tag{1.21}$$

Since the spatial variables are integrated in formula (1.16), this formula can be written in the form of (1.21):

$$\Phi(\boldsymbol{r}, \omega) = F(\omega) \int_{S_0} G(\boldsymbol{r}, \boldsymbol{r}_0) u_0(\boldsymbol{r}_0)\, d\sigma^0, \tag{1.22}$$

and in a specific case for a half-space

$$\Phi(\boldsymbol{r}, \omega) = \frac{F(\omega)}{2\pi} \int_{S_0} \frac{\exp(ik|\boldsymbol{r} - \boldsymbol{r}_0|)}{|\boldsymbol{r} - \boldsymbol{r}_0|} u_0(\boldsymbol{r}_0)\, d\sigma^0. \tag{1.23}$$

Formulae (1.22) and (1.23) permit some very important conclusions to be drawn. Considering that the wave number $k = \omega/c$ it can be seen that the integral

$$\Phi_s(\boldsymbol{r}, \omega) = \int_{S_0} G(\boldsymbol{r}, \boldsymbol{r}_0) u_0(\boldsymbol{r}_0)\, d\sigma^0 \tag{1.24}$$

or the integral

$$\Phi_s(\boldsymbol{r}, \omega) = \frac{1}{2\pi} \int_{S_0} \frac{\exp\left(i \frac{\omega}{c} |\boldsymbol{r} - \boldsymbol{r}_0|\right)}{|\boldsymbol{r} - \boldsymbol{r}_0|} u_0(\boldsymbol{r}_0)\, d\sigma^0 \tag{1.25}$$

represent the spatial distribution of the acoustic field of a harmonic wave as determined from the amplitude distribution such as the spatial pulse distribution $u_0(\boldsymbol{r}_0)$. In addition $\Phi_s(\boldsymbol{r}, \omega)$ can be replaced with all solutions of the Huyghens integral formula (1.24) known from harmonic wave acoustics. Knowing $\Phi_s(\boldsymbol{r}, \omega)$ this value should be multiplied by the transform $F(\omega)$ of the time behaviour, achieving the acoustic potential transform of a real pulse field

$$\Phi(\boldsymbol{r}, \omega) = F(\omega) \Phi_s(\boldsymbol{r}, \omega). \tag{1.26}$$

Such a simplification is valid only when formula (1.19) can be used.

The potential of the acoustic field is determined as the inverse Fourier transform of formula (1.26), i.e. this potential is given as the integral [1]

$$\Phi(\boldsymbol{r}, t) = \frac{1}{\sqrt{2\pi}} \int_{-\infty}^{\infty} F(\omega)\Phi_s(\boldsymbol{r}, \omega)\exp(i\omega t)d\omega. \tag{1.27}$$

In the case when the source receives a pulse in the form of the Dirac distribution $\delta(t)$ and in view of the fact that the Fourier transform of this pulse has a value of unity [1]:

$$F_D(\omega) = 1, \tag{1.28}$$

the potential of the acoustic field is given directly in the form of the integral

$$\varphi_D(\boldsymbol{r}, t) = \int_{-\infty}^{\infty} \Phi_s(\boldsymbol{r}, \omega)\exp(i\omega t)d\omega. \tag{1.29}$$

Formula (1.29) indicates that all acoustic fields calculated for harmonic waves can be regarded as Fourier transforms for Dirac pulses while integral (1.29) transforms it into the field of these pulses.

It should be pointed out that the above train of thought is most general and can be applied to any acoustic field, also including fields of diffracted waves.

In considering the problems in wave diffraction by an obstacle two specific cases can be distinguished, i.e. an ideal rigid obstacle on which, S_p, the summary acoustic field, which is the field of incident and reflected waves, satisfies the condition [16]

$$\left(\frac{\partial \varphi_s}{\partial n}\right)_{S_p} = 0, \tag{1.30}$$

and an ideal compliant obstacle on which the summary acoustic field gives zero acoustic pressure. For harmonic waves this is equivalent to the condition [13], [16]

$$\varphi = 0 \quad \text{on } S_p. \tag{1.31}$$

In the case of pulses the relavant condition (1.31) has the form [16]

$$p = \varrho \frac{\partial \varphi}{\partial t} = 0 \quad \text{on } S_p, \tag{1.32}$$

i.e., in view of the fact that ϱ denotes here the density of the medium in rest, there is the condition

$$\frac{\partial \varphi}{\partial t} = 0 \quad \text{on } S_p. \tag{1.33}$$

In a general case there is the so-called impedance condition. Designating as z^0 the impedance of the obstacle surface by which waves are diffracted, according to the definition of acoustic impedance [13], [16],

$$\frac{p}{u} = \varrho \frac{(\partial\varphi/\partial t)_{S_0}}{(\partial\varphi/\partial n)_{S_0}} = z_p(x_i, \omega). \tag{1.34}$$

In a general case, the acoustic impedance on the diffracting surface can be a function of position and frequency, whereas the acoustic field on the surface should be such that p/u is independent of time, which would limit the class of pulses for which the diffraction problem can be solved with general impedance conditions.

Wishing to apply the concept given at the beginning of this section to diffraction problems, i.e. wishing to regard the potential of the harmonic field of diffracted waves as the Fourier transform of the pulse (after multiplication by $F(\omega)$), one must first investigate the boundary conditions for this transform. In view of the fact that the impedance conditions occur infrequently, the previous order will be retained, i.e. ideal rigid, compliant and, finnally, "impedance" surfaces will be considered in that succession. From formula (1.15) condition (1.30), after Fourier transformation, in view of the additivity of the transforms, requires that the following equation should occur for the summary acoustic field,

$$\frac{\partial \Phi_s}{\partial n} = 0 \quad \text{on } S_p \tag{1.35}$$

for an ideal rigid surface. In turn on the ideal compliant surface the derivative $\partial\varphi_s/\partial t$ undergoes Fourier transformation, i.e., in view of formula (1.8), there is the condition [1]

$$\Phi_s = 0 \quad \text{on } S_p. \tag{1.36}$$

It can be seen that in the two specific cases, infinitely rigid and infinitely compliant wave diffracting obstacles, the boundary conditions for the transform are the same as those for the acoustic potential of harmonic waves. This permits any acoustic field of diffracted harmonic waves to be treated as the field of the pulse transform Φ_s, which when multiplied by the transform of the time behaviour $F(\omega)$ gives the transform of the diffracted pulse field and the desired acoustic field in the form of integral (1.27) or integral (1.29) for the Dirac pulse.

For the impedance condition (1.34)

$$\varrho \left(\frac{\partial \varphi}{\partial t}\right)_{S_p} = z_p(x_i, \omega) \left(\frac{\partial \varphi}{\partial n}\right)_{S_p}. \tag{1.37}$$

In formula (1.37) both the acoustic potential φ and its derivatives $(\partial\varphi/\partial t)_{S_p}$ and $(\partial\varphi/\partial n)_{S_p}$ are time functions, whereas the impedance of the surface is

independent of time. A direct Fourier transform of equation (1.37) gives

$$\varrho \int_{-\infty}^{\infty} \left(\frac{\partial \varphi s}{\partial t}\right)_{S_p} \exp(-i\omega t)\,dt = z_p(x_i, \omega) \int_{-\infty}^{\infty} \left(\frac{\partial \varphi s}{\partial n}\right)_{S_p} \exp(-i\omega t)\,dt. \quad (1.38)$$

In formula (1.38) the impedance, as it is independent of time, was moved before the integral sign.

From formulae (1.8) and (1.15), formula (1.38) becomes

$$\omega \varrho \Phi_s(x_i, \omega) = i z_p(x_i, \omega)\, U_{os}(x_i, \omega), \quad (1.39)$$

i.e.

$$\frac{\varrho \Phi_s(x_i, \omega)}{U_{os}(x_i, \omega)} = \frac{i}{\omega} z_p(x_i, \omega). \quad (1.40)$$

Formula (1.34) which represents the impedance condition takes in the case of a harmonic wave the form ((1.32) for $\varphi(x_i, t) = \varphi(x_i)\exp(-i\omega t)$)

$$\frac{\varrho \varphi(x_i)}{u_0(x_i)} = \frac{i}{\omega} z_p(x_i), \quad (1.41)$$

i.e. the same as (1.40).

In all cases the boundary conditions are the same for transforms as those for the acoustic potential, permitting the pulses from the diffracted acoustic fields of harmonic waves to be determined by the present acoustic field method. This approach facilitates to a large extent the solution of the problems of pulse diffraction by obstacles of different shape, and when the solution for harmonic waves is known the pulse field is obtained in the form of a single integral (1.27) which can be evaluated analytically or numerically.

3. Applications of the theory

The theory given in section 1 can be illustrated by such a large number of examples that this would exceed the range of the present paper. In principle it is enough to multiply all solutions for a harmonic acoustic field by the transform of the relevant pulse and as a result the transform of the pulse field potential can be achieved.

Since, as it was already mentioned, various integral transformations have been used to solve the problem of wave diffraction by a wedge, only a few examples will be given here to illustrate direct source radiation.

1. A system of two point sources distance d (Fig. 2) apart will be given as the first example. Both of the sources receive the same Dirac pulse δ at a time $t = \tau$. The acoustic field distribution in the far field will now be investigated. The vibration velocity amplitude in the formula of the far field potential can be

assumed to have a value of unity. The formula for a harmonic wave [13], [16] can be written directly as the formula of the transform for the Dirac pulse

$$\Phi_D(P,t) = \frac{\exp\left(-i\frac{\omega}{c}r_0\right)}{r_0}\exp\left(i\frac{\omega d}{2c}\sin\gamma\right)\cos\left(\frac{\omega d}{2c}\sin\gamma\right). \tag{2.1}$$

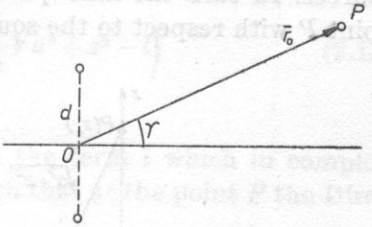

Fig. 2. A system of two point sources

The acoustic potential can be achieved as the inverse transform of [2.1], i.e. given by the integral

$$\varphi_D(P,t) = \frac{1}{r_0}\int_{-\infty}^{\infty}\exp\left[i\omega\left(\frac{d}{2c}\sin\gamma - \frac{r_0}{c} + t\right)\right]\cos\left(\frac{\omega d}{2c}\sin\gamma\right)d\omega. \tag{2.2}$$

In integration of (2.2) only the even part remains, i.e.

$$\varphi_D(P,t) = \frac{2}{r_0}\int_0^{\infty}\cos\omega\left(\frac{d}{c}\sin\gamma - \frac{r_0}{c} + t\right)d\omega + \frac{1}{r_0}\int_0^{\infty}\cos\left(\frac{\omega d}{2c}\sin\gamma\right)d\omega. \tag{2.3}$$

The use of the formula of cosine product in the subintegral expression gives [3]

$$\varphi_D(P,t) = \frac{1}{r_0}\int_0^{\infty}\cos\omega\left(\frac{d}{c}\sin\gamma - \frac{r_0}{c} + t\right)d\omega + \frac{1}{r_0}\int_0^{\infty}\cos\omega\left(\frac{r_0}{c} - t\right)d\omega. \tag{2.4}$$

The two integrals represent the Dirac distribution, according to the formula [2]

$$\int_0^{\infty}\cos(ax)dx = \pi\delta(a). \tag{2.5}$$

Finally,

$$\varphi_D(P,t) = \frac{\pi}{r_0}\delta\left(\frac{d}{c}\sin\gamma - \frac{r_0}{c} + t\right) + \frac{\pi}{r_0}\delta\left(\frac{r_0}{c} - t\right). \tag{2.6}$$

It can be seen that at the point P of the far field the Dirac pulse δ occurs twice, i.e. at a time t_1:

$$t_1 = \frac{r_0}{c} - \frac{d}{c}\sin\gamma \tag{2.7}$$

and at a time t_2:

$$t_2 = \frac{r_0}{c}. \tag{2.8}$$

The time t_2 is the time required for the pulse to reach the point P from the centre of the system, i.e. from the point 0 on the section d between the sources. In turn the time t_1 is caused by the asymmetry of the position of the point P with respect to the sources, and in the case when $\gamma = 0$ $t_1 = t_2 = r_0/c$.

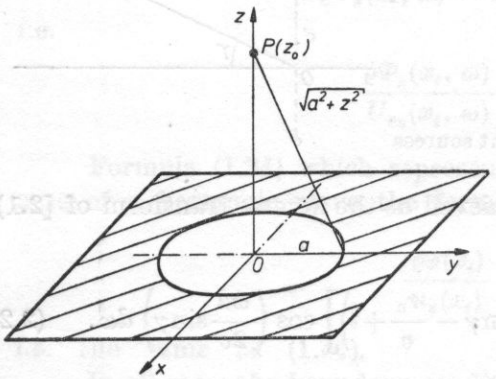

Fig. 3. The piston in the baffle

2. Another example is provided by the near field on the so-called axis of the acoustic system consisting of a rigid piston, i.e. a piston which vibrates all over its surface, placed in an infinite, rigid baffle (Fig. 3), when it receives a Dirac pulse. Assuming the vibration velocity amplitude in the formula of the harmonic solution to have a value of unity, the near field expression [13], [16] can be given in the form of the transform of the Dirac pulse

$$\Phi_D(z, \omega) = 2\varrho c \exp\left[-i\frac{\omega}{2c}(\sqrt{a^2+z^2}+z)\right]\sin\left[\frac{\omega}{2c}(\sqrt{a^2+z^2}-z)\right]. \tag{2.9}$$

The acoustic potential itself on the z axis thus becomes

$$\varphi(z, t) = 2\varrho c \int_{-\infty}^{\infty} \exp\left[-i\frac{\omega}{2c}(\sqrt{a^2+z^2}+z)\right]\sin\left[\frac{\omega}{2c}(\sqrt{a^2+z^2}-z)\right]\exp(i\omega t)\,d\omega. \tag{2.10}$$

Like in the previous case, in integration only the even component remains and therefore

$$\varphi(z, t) = -2i\int_0^{\infty} \sin\left[\frac{\omega}{2c}(\sqrt{a^2+z^2}+z)-\omega t\right]\sin\left[\frac{\omega}{2c}(\sqrt{a^2+z^2}-z)\right]d\omega. \tag{2.11}$$

The use of the formula of cosine product on the left of (2.11) [3] gives

$$\varphi(z,t) = -i\int_0^\infty \cos\omega\left(\frac{z}{c}-t\right)d\omega + i\int_0^\infty \cos\omega\left(\frac{1}{c}(\sqrt{a^2+z^2}-t\right)d\omega. \tag{2.12}$$

Using formula (2.5) again

$$\varphi(z,t) = -i\pi\delta\left(\frac{z}{c}-t\right)+i\pi\delta\left(\frac{1}{c}\sqrt{a^2+z^2}-t\right) \tag{2.13}$$

(see formula (17) in [14]).

This result is very interesting. Apart from the term i which in complex number notation denotes phase shift, it can be seen that at the point P the Dirac pulse occurs twice, namely after the time t_1:

$$t_1 = \frac{z}{c} \tag{2.14}$$

– this is a pulse coming from the centre of the piston and after the time t_2:

$$t_2 = \frac{\sqrt{a^2+z^2}}{c}. \tag{2.15}$$

The time t_2 is the time required for a pulse from the circumference of the piston to reach the point P. The action of the piston at all points P in the near field can be reduced to the superposition of the pulse from the centre and the one from the circumference.

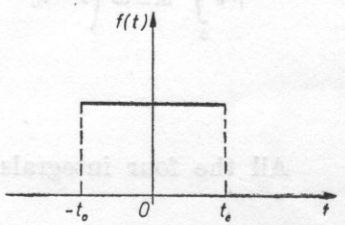

Fig. 4. The shape of the rectangular pulse

3. The final example to be considered here is a piston which is the same as that in example 2, but which receives a rectangular pulse (Fig. 4) with height of unity and active from $t = -t_0$ to $t = t_0$. The function $f(t)$ is here the distribution

$$\mathrm{f}(t) = \begin{cases} 1, & -t_0 \leqslant t \leqslant t_0 \\ 0, & t < -t_0; t > t_0. \end{cases} \tag{2.16}$$

In view of the symmetry of $f(t)$ the transform $F(\omega)$ can be written in the form of the so-called cosine transform [1]

$$F(\omega) = \int_0^\infty f(t)\cos(\omega t)\,dt = \frac{2\sin(\omega t_0)}{\omega}. \tag{2.17}$$

From formula (1.26) the acoustic potential transform becomes

$$\Phi(z, \omega) = \frac{2\sin(\omega t_0)}{\omega} \exp\left[-i\frac{\omega}{2c}(\sqrt{a^2+z^2}+z)\right]\sin\left[\frac{\omega}{2c}(\sqrt{a^2+z^2}-z)\right], \tag{2.18}$$

whereas the acoustic potential itself on the z axis takes the form of the transform inverse to (2.18):

$$\varphi(z, t) = 2c\int_{-\infty}^{+\infty} \frac{\sin(\omega t_0)}{\omega} \exp\left[-i\omega\left(\frac{\sqrt{a^2+z^2}}{c}-t\right)\right]\sin\left[\frac{\omega}{2c}(\sqrt{a^2+z^2}-z)\right]d\omega. \tag{2.19}$$

Considering the odd and even form of the subintegral function

$$\varphi(z, t) = 4i\int_0^\infty \frac{\sin(\omega t_0)}{\omega}\sin\left[\omega\left(t-\frac{\sqrt{a^2+z^2}+z}{2c}\right)\right]\sin\left[\frac{\omega}{2c}(\sqrt{a^2+z^2}-z)\right]d\omega. \tag{2.20}$$

The use of the formula of triple sine product [3] gives

$$\varphi(z, t) = i\int_0^\infty \sin\omega\left(t+t_0-\frac{1}{c}\sqrt{a^2+z^2}\right)\frac{d\omega}{\omega}+$$

$$+i\int_0^\infty \sin\omega\left(t-t_0-\frac{z}{c}\right)\frac{d\omega}{\omega}-i\int_0^\infty \sin\omega\left(t-t_0+\frac{1}{c}\sqrt{a^2+z^2}\right)\frac{d\omega}{\omega}+$$

$$+i\int_0^\infty \sin\omega\left(t-t_0-\frac{z}{c}\right)\frac{d\omega}{\omega}. \tag{2.21}$$

All the four integrals have the form [3]

$$\int_0^\infty \sin_\omega(m\omega)\,d\omega = \begin{cases} \dfrac{\pi}{2}, & m>0, \\ 0, & m=0, \\ -\dfrac{\pi}{2}, & m<0. \end{cases} \tag{2.22}$$

It follows from the analysis of the value of the individual integrals that they reduce so that the gate pulse does not occur at the point P until the time $(z/c)-t_0$ and lasts till the time $(\sqrt{a^2+z^2}/c)-t_0$.

References

[1] H. BATEMAN, *Tables of integral transforms*, **1**, McGraw Hill New York-London 1954.

[2] A. S. DAWYDOW, *Quantum mechanics* (in Polish), PWN, Warsaw 1967 (*Mathematical supplement*).

[3] H. B. DWIGHT, *Tables of integrals and other mathematical data*, Macmillan, New York 1961, 4th ed.

[4] F. G. FRIEDLANDER, *The diffraction of sound pulses*, I. *Diffraction by a semi infinite plane*, Proc. Roy. Soc. London, 186, 322-344 (1946).

[5] F. G. FRIEDLANDER, *The diffraction of sound pulses*, II. *Diffraction by an infinite wedge*, Proc. Roy. Soc. London, 186, 344-351 (1946).

[6] M. C. JUNGER, M. PARULI, *Elements d'acoustique physique*, Malaine S. A. Paris 1978.

[7] I. KAY, *The diffraction of an arbitrary pulse by a wedge*, Comm. Pure Appl. Math., 6, 419-434 (1953).

[8] J. B. KELLER, A. BRANCK, *Diffraction and reflection of pulses by wedges and corners*, Comm. Pure. Appl. Math., 4, 75-94 (1951).

[9] J. W. MILES, *On the diffraction of an acoustic pulse by a wegde*, Proc. Roy. Soc. London, *A* 212, 544-547 (1952).

[10] J. W. MILES, *The diffraction of an electromagnetic pulse by a wedge*, Proc. Roy. Soc. London, *A* 212, 547-551 (1952).

[11] F. OBERHETTINGER, *On the propagation of pulses*, I. *diffraction of pulses by wedges*, Zeitschrift für Physik, Bd, 146, 423-435 (1956).

[12] F. OBERHETTINGER, *On the diffraction and reflection of waves and pulses by wedges and corners*, Journal of Research of the National Bureau of Standards, **61**, 5, 343-365 (1958).

[13] E. SKUDRZYK, *The foundations of acoustics*, Springer Verlag, Wien-New York 1971.

[14] P. STEPANISHEN, *Transient radiation from pistons in an infinite planar baffle*, J. Acoust. Soc. Am., **49**, 5 (2), 1629-1638 (1971).

[15] R. D. TURNER, *The diffraction of a cylindrical pulse by halfplane*, Quart. Appl. Math., **14**, 63-73 (1956).

[16] R. WYRZYKOWSKI, *Linear theory of the acoustic field of gaseous media* (in Polish), WSP, Rzeszów 1972.

Received on 1 March, 1983

C H R O N I C L E

A BRIEF REPORT ON WORKSHOP ON ULTRASOUND THERAPY AND ULTRASONIC POWER MEASUREMENT

A one day Workshop and Exhibition on Ultrasound Therapy and Ultrasonic Power Measurement was organised on 14th Feb. 1983 by Ultrasonic Society of India (USI) in collaboration with National Physical Laboratory, New Delhi and Delhi Productivity Council at National Physical Laboratory, New Delhi-110012. The purpose of the Workshop was to discuss the significance of calibration procedures of ultrasonic power output and frequency for therapeutic applications by bringing together the medical doctors, physicists, and engineers on a common forum. The subjects covered in the workshop included various aspects of ultrasonic therapy, calibration procedures for characterizing output of therapeutic devices and the most important of all were the future recommendations.

The Workshop was inaugurated by Dr. A. R. VERMA, Jawaharlal Nehru Fellow and Patron of the Ultrasonic Society of India. Dr. C. R. HILL, Head of the Dept. of Medical Physics, Institute of Cancer Research, U. K. and Dr. K. BRENDEL, Head of Ultrasonics, PTB, West Germany, delivered invited talks on the subject. More than fifty scientists including the foreigners attended the Workshop.

In total eight papers were presented in two sessions. The forenoon session was devoted to the therapeutic effect of the ultrasound and the afternoon one to the measurements of parameters relevant to ultrasonic therapy. The presentation of the papers was followed by panel discussion on *The significance of calibration of ultrasonic power output for therapeutic equipment.*

The important recommendations of the panel were as follows:

1. Teaching courses should be held for the training of the doctors in the calibration procedures for therapeutic equipment with a special emphasis on significance of this practice.

2. Portable and rugged ultrasonic power meter should be developed for calibration output of therapy units for use in hospital.

3. Detailed studies on the bioeffects of therapeutic ultrasound should be carried out in order to make treatment by ultrasonic therapy more effective.

V. N. Bindal (New Delhi)